# A salt bridge-mediated resistance mechanism to FtsZ inhibitor PC190723 revealed by a cell-based screen

Ajay Kumar Sharma[1,2,3], Sakshi Mahesh Poddar[1,2,3], Joyeeta Chakraborty[4], Bhagyashri Soumya Nayak[1,2,3], Srilakshmi Kalathil[1,2,3], Nivedita Mitra[1,2,3], Pananghat Gayathri[4‡] and Ramanujam Srinivasan[1,2,3‡]

[1] School of Biological Sciences, National Institute of Science Education and Research, Bhubaneswar – 752050, India

[2] Homi Bhabha National Institutes (HBNI), Training School Complex, Anushakti Nagar, Mumbai, India 400094

[3] Centre for Interdisciplinary Sciences, National Institute of Science Education and Research, Bhubaneswar, India 752050

[4] Biology, Indian Institute of Science Education and Research, Pune – 411008, India

[‡] Corresponding authors

e-mail: rsrini@niser.ac.in; gayathri@iiserpune.ac.in

**Abstract:**

Bacterial cell division proteins, especially the tubulin homolog FtsZ, have emerged as strong targets for developing new antibiotics. Here, we have utilized the fission yeast heterologous expression system to develop a cell-based assay to screen for small molecules that directly and specifically target the bacterial cell division protein FtsZ. The strategy also allows for simultaneous assessment of the toxicity of the drugs to eukaryotic yeast cells. As a proof-of-concept of the utility of this assay, we demonstrate the effect of the inhibitors sanguinarine, berberine and PC190723 on FtsZ. Though sanguinarine and berberine affect FtsZ polymerization, they exert a toxic effect on the cells. Further, using this assay system, we show that PC190723 affects *Helicobacter pylori* FtsZ function and gain new insights into the molecular determinants of resistance to PC190723. Based on sequence and structural analysis and site-specific mutations, we demonstrate that the presence of salt-bridge interactions between the central H7 helix and beta-strands S9 and S10 mediate resistance to PC190723 in FtsZ. The single-step *in vivo* cell-based assay using fission yeast enabled us to dissect the contribution of sequence-specific features of FtsZ and cell permeability effects associated with bacterial cell envelopes. Thus, our assay serves as a potent tool to rapidly identify novel compounds targeting polymeric bacterial cytoskeletal proteins like FtsZ to understand how they alter polymerization dynamics and address resistance determinants in targets.

**Running Title:** Salt bridge interactions in FtsZ mediate resistance to PC190723

**Keywords:** FtsZ, PC190723, antimicrobial resistance, bacterial cytoskeleton, fission yeast

**Introduction:**

43 The rapid emergence and spread of antibiotic resistance to almost every antibiotic
44 currently in use against bacteria, has resulted in an urgent need to develop new classes of
45 antibiotics. Among the new targets with a novel mechanism of action to overcome the
46 emerging resistance problem (Butler and Paterson 2020), one of the most potential target
47 candidates is FtsZ, an essential bacterial cell division machinery protein (Silber et al. 2020;
48 Wang et al. 2003; Schaffner-Barbero et al. 2012; Carro 2019; Zorrilla et al. 2021; Tripathy
49 and Sahu 2019; Andreu et al. 2022). FtsZ is a prokaryotic homolog of tubulin, which is
50 highly conserved and present in all bacteria and many archaea (Addinall and Holland
51 2002; Vaughan et al. 2004; Erickson et al. 2010; Erickson 1995; Margolin 2005; Nogales et
52 al. 1998). FtsZ monomers self-assemble into polymeric structures in presence of GTP to
53 give rise to FtsZ protofilaments *in vitro* and assemble into the so-called Z-ring at the
54 division site *in vivo*. The Z- ring is the first structure to be assembled at the division site
55 and is responsible for the recruitment of more than a dozen other accessory proteins,
56 which comprise the divisome, the division apparatus of the cell (Bi and Lutkenhaus 1991;
57 Ma et al. 1996; Weiss et al. 1999; Weiss 2004; Huang et al. 2013; RayChaudhuri and Park
58 1992; Bramhill and Thompson 1994). The Z-ring is a highly dynamic structure with a half-
59 life of less than 10 seconds due to the constant exchange of FtsZ molecules between the
60 ring and the soluble monomers (Anderson et al. 2004). Since the Z-ring lies at the core of
61 the cell division process, its functional defects result in bacterial growth inhibition and cell
62 death (Vollmer 2006; Zorrilla et al. 2021; Mahone and Goley 2020; Barrows and Goley
63 2021; Addinall and Lutkenhaus 1996).

64 FtsZ has three important protein pockets that bind small molecules and are
65 collectively known as druggable regions. These regions are the nucleotide-binding domain
66 (NBD), the inter-domain cleft (IDC) present between the central core helix (H7 helix) and
67 the C- terminal domain (CTD) and the T7 loop (Löwe and Amos 1998; Kusuma et al. 2019;

68 Andreu et al. 2022). The T7 loop of one subunit is inserted into the NBD of another
69 subunit of FtsZ to form a catalytic site for GTP hydrolysis. Several compounds have been
70 evaluated for their activity against FtsZ from both Gram-positive bacteria and Gram-
71 negative bacteria. Although many exhibited only weak activity *in vivo* against Gram-
72 negative bacteria, derivatives could be promising. These include benzamides (Haydon et
73 al. 2008; Adams et al. 2011; Straniero et al. 2017, 2020a), trisubstituted benzimidazoles
74 (Kumar et al. 2011), 4-bromo-1*H*-indazole derivatives (Wang et al. 2015), cinnamaldehyde
75 and its derivatives (Domadia et al. 2007; Li et al. 2015), curcumin (Rai et al. 2008),
76 heterocyclic molecules like guanidinomethyl biaryl compounds (Kaul et al. 2012),
77 pyrimidine-quinuclidine scaffolds (Chan et al. 2013), 3-phenyl substituted 6,7-
78 dimethoxyisoquinoline (Kelley et al. 2012), thiazole orange derivatives (Sun et al. 2017),
79 viriditoxin (Wang et al. 2003), N-heterocycles such as zantrins and derivatives (Margalit et
80 al. 2004; Nepomuceno et al. 2015).
81 Berberine and sanguinarine are plant-derived benzylisoquinoline alkaloids, with
82 antibacterial activity (Wolff and Knipling 1993; Pierpaoli et al. 2021; Cernáková and
83 Kostálová 2002; Chu et al. 2016). Berberine binds to FtsZ at a 1:1 ratio *in vitro* and
84 exhibits dose-dependent inhibition of FtsZ assembly kinetics with a reduction in GTPase
85 activity. Berberine is believed to target the GTP-binding pocket in the FtsZ structure and
86 further affects the FtsZ polymer stability and Z- ring formation *in vivo* (Boberek et al. 2010;
87 Domadia et al. 2008; Sun et al. 2014; Pradhan et al. 2021). Sanguinarine, also thought to
88 bind the nucleotide-binding domain (NBD) in FtsZ, prevents the bundling of FtsZ
89 protofilaments *in vitro* and perturbs the Z- ring assembly *in vivo* (Beuria et al. 2005). The
90 precise mechanism of inhibition or the binding site of these inhibitors remains unclear.
91 The most potent and promising among the FtsZ inhibitors is PC190723, a 2,6-
92 difluorinated 3-methoxybenzamide derivative, as it has proven to be efficacious in *in vivo*
93 model of mice infected with a lethal dose of *Staphylococcus aureus* (Haydon et al.

94 2008). Crystal structures of FtsZ from *S. aureus* with PC190723 reveal binding at the
95 inter-domain cleft between the central core helix (H7 helix) and the C-terminal domain
96 (CTD) of FtsZ (Matsui et al. 2012a; Tan et al. 2012) and is the only inhibitor whose target
97 site in FtsZ is clearly established. PC190723 binds preferentially to the T state of *S.*
98 *aureus* FtsZ in which the cleft is opened, thus stabilizing the high-affinity conformation
99 required for FtsZ polymer elongation (Matsui et al. 2012a; Fujita et al. 2017). Thereby,
100 PC190723 reduces the critical concentration for polymerization and induces FtsZ
101 assembly (Andreu et al. 2010; Elsen et al. 2012). Although the resistance of streptococci,
102 enterococci and many Gram-negative bacteria to PC190723 (Haydon et al. 2008; Kaul et
103 al. 2013b) and poor drug and pharmacokinetic properties have hampered the pre-clinical
104 trials with PC190723 (Stokes et al. 2013; Kaul et al. 2013a), phase-I tests are in progress
105 by TAXIS pharmaceuticals (Monmouth Junction, NJ, USA) for the benzamide class of drug
106 TXA709 (Butler and Paterson 2020; TAXIS Pharmaceuticals 2020).
107 Thus, despite several years of intense research on FtsZ inhibitors, a commercially
108 viable antibiotic that targets FtsZ is not yet available. One of the major hindrances has
109 been the validation that FtsZ is the actual direct target of these small molecule compounds
110 (Kusuma et al. 2019; Zorrilla et al. 2021; Schaffner-Barbero et al. 2012). Although several
111 other small molecules have been shown to inhibit bacterial cell division, presumably by
112 directly inhibiting FtsZ function, many of them have also been shown to be due to indirect
113 effects on membranes (Hurley et al. 2016). Several methods have been used to ascertain
114 FtsZ as the target of the drug, and the various approaches have been reviewed in detail by
115 many (Kusuma et al. 2019; Silber et al. 2020; Zorrilla et al. 2021; Andreu et al.
116 2022). Andreu et al. (2022) have recently proposed a streamlined experimental protocol
117 for the screening and characterization of FtsZ inhibitors. A scheme of methods to be
118 followed, from the identification of hit compounds to the development of a lead compound,
119 has also been proposed. These include several assays for monitoring effects on FtsZ

120 polymerization, cytological effects on eukaryotic cells, pharmacological properties and
121 structural optimization (Andreu et al. 2022; Schaffner-Barbero et al. 2012). Any small
122 molecule antagonist identified thus should have no off-target effects and minimally affect
123 eukaryotic cells. A single-step screening method that identifies small molecules, directly
124 targeting FtsZ assembly and as well as selects out compounds probably toxic to
125 eukaryotic cells would be ideal. Moreover, the screen should be easily scalable to high-
126 throughput platforms.

127 We had previously established *Schizosaccharomyces pombe* as a useful model
128 system to study bacterial cytoskeletal proteins. We had shown that A22, a small molecule
129 inhibitor of the actin homologue, MreB, prevented its polymerization in yeast cells as well
130 (Srinivasan et al. 2007). Further, we reported that FtsZ assembles into ring-like structures
131 with similar characteristics to Z-rings in bacterial cells when expressed in *S. pombe* or
132 *Saccharomyces cerevisiae* (Srinivasan et al. 2008). Moreover, the dynamics of chloroplast
133 FtsZs have also been successfully studied using the heterologous fission yeast expression
134 system (TerBush and Osteryoung 2012; Yoshida et al. 2016; TerBush et al. 2018). These
135 observations prompted us to explore if the heterologous expression system using *S.*
136 *pombe* could serve as a platform for testing and screening chemical compounds targeting
137 FtsZ directly.

138 In this study, we show that FtsZ from two pathogenic bacterial species, *S. aureus*
139 and *Helicobacter pylori*, expressed in fission yeast, assemble into dynamic ring-like and
140 spiral polymers, respectively. We test the effect of known small molecule inhibitors of
141 FtsZ, sanguinarine, berberine and PC190723 on the assembly of FtsZ polymers. Herein,
142 we thus develop a proof-of-concept of a cell-based screening method that is easily
143 scalable to existing high-throughput platforms. The method combines the ability to
144 establish the specificity of the target by directly assaying the polymerization of FtsZ in the
145 cellular milieu without a tedious protein purification step, as well as assessing toxicity to

146 yeast cells in a single step. We find that although sanguinarine and berberine affected
147 FtsZ polymerization, they also affected yeast cell physiology. We show that while all three
148 inhibitors exert an effect on FtsZ assembly, PC190723 specifically promotes the assembly
149 of FtsZ polymers of *S. aureus* and *H. pylori*. Further, we probed the determinants of
150 resistance to PC190723. Based on FtsZ sequence and structure analysis, we show that
151 salt-bridge interactions between the central H7 helix and S9 / S10 β-sheet prevent the
152 inhibitor from accessing the inter-domain cleft (IDC). This appears to be a sequence-
153 determined resistance probably prevalent in many Gram-negative bacteria. We thus
154 demonstrate the utility of the heterologous yeast system (*S. pombe*) for identifying
155 chemical compounds directly targeting FtsZ, evaluating them for toxicity to eukaryotic cells
156 and studying the molecular determinants of drug resistance.
157

158 **Results:**

159 ***S. aureus and H. pylori FtsZ assemble into polymeric structures in fission yeast***

160 We expressed FtsZ from two pathogenic species, *S. aureus* and *H. pylori* (hereafter
161 referred to as SaFtsZ for *S. aureus* FtsZ and HpFtsZ for *H. pylori* FtsZ, respectively) as C-
162 terminal GFP fusions in *S. pombe*. Expression of FtsZ in *S. pombe* was achieved from a
163 pREP42-GFP vector (a medium strength thiamine repressible promoter *nmt41/42*
164 containing vector; (Basi et al. 1993; Moreno et al. 2000) by growing cultures in minimal
165 medium in the absence of thiamine (induction medium) as reported earlier (Srinivasan et
166 al. 2008). Epifluorescence microscopy showed that SaFtsZ assembled predominantly into
167 spot-like structures (**Fig. 1A**) and were similar in appearance to that assembled by FtsZ
168 from *Escherichia coli* (EcFtsZ) **(Fig. 1B)**. Assembly of SaFtsZ into ring-like structures was
169 only discernible by super-resolution microscopy using structural illumination (3D-SIM) **(Fig.
170 1C)**, whereas ring-like structures of EcFtsZ were visualized by deconvolution of images
171 **(Fig. 1B iii)**. Interestingly, HpFtsZ assembled into linear cable-like structures as well as

172 twisted polymers that were curled and spiral in appearance **(Fig. 1D)**. The spiral filaments
173 were more clearly visualized by deconvolution of the images (**Fig. 1D iii and 1E**). Further,
174 super-resolution imaging using 3D-SIM clearly revealed that HpFtsZ assembles into spiral
175 filaments in fission yeast (**Fig. 1F**). Spiral polymers appeared early, at 16 – 18 hours after
176 induction of expression (absence of thiamine), and linear cables appeared later at 20 – 22
177 hours **(Fig. S1)**. The smooth linear polymers possibly arise from lateral association and
178 bundling of FtsZ filaments (Monahan et al. 2009), but the factors determining the two forms
179 in yeast cells remain unclear.

180 We had previously shown that the diameter of EcFtsZ rings assembled in yeast
181 were 0.48 ± 0.042 μm (SEM ± SD) (Srinivasan et al. 2008). Quantification of the diameter
182 of the rings assembled by SaFtsZ revealed that they had a mean diameter of 0.29 ± 0.04
183 μm (SEM ± SD) and were thus smaller than EcFtsZ rings **(Fig. S2A)**. The spiral polymers
184 of HpFtsZ had a mean diameter of 0.35 ± 0.01 μm and a pitch of 0.41 ± 0.03 μm (SEM ±
185 SD) **(Fig. S2B i and ii)**. These results show that FtsZ from both species *S. aureus*
186 (SaFtsZ) and *H. pylori* (HpFtsZ), when expressed in fission yeast cells, assemble into
187 polymeric structures like many other FtsZs.

188

189 ***Sanguinarine and berberine prevent FtsZ assembly in fission yeast but also affect***
190 ***yeast cell morphology***

191 Sanguinarine and berberine have been shown to perturb FtsZ ring assembly in *E.*
192 *coli* (Beuria et al. 2005; Boberek et al. 2010; Domadia et al. 2008; Liu et al.
193 2017). Although sanguinarine has been reported to inhibit septation and cell division in *S.*
194 *aureus* (Obiang-Obounou et al. 2011), its effects on SaFtsZ or HpFtsZ have not yet been
195 reported. We, therefore, tested if any of these molecules exhibited any direct effects on
196 FtsZ expressed in yeast cells. Fission yeast cultures were grown at 30ºC in the absence
197 of thiamine for 10 – 12 hours to induce the expression of the bacterial FtsZ-GFP fusions.

198 DMSO or drugs were subsequently added to the cultures and further grown at 30ºC for
199 another 10 – 12 hours prior to imaging.

200 A microscopic examination of fission yeast cells expressing SaFtsZ **(Fig. 2A)**,
201 EcFtsZ **(Fig. 2B)** or HpFtsZ **(Fig. 2C)** in the presence of sanguinarine **(Fig. 2 A ii – C ii)** or
202 berberine **(Fig. 2 A iii – C iii)** revealed that assembly of FtsZ into polymers was inhibited in
203 the presence of the drugs as compared to untreated (DMSO added) cells **(Fig. 2 A i – C**
204 **i)**. A significant reduction in the percentage of cells that exhibited FtsZ assemblies (spots/
205 dots in the case of SaFtsZ or EcFtsZ and filaments in the case of HpFtsZ) in the presence
206 of sanguinarine or berberine as compared to control untreated cells **(Fig. 2 D i – iii and F i**
207 **– iii)** was observed (≥ 500 cells counted for each replicate; N = 3). To obtain a quantitative
208 measure of the effect of drugs on FtsZ assembly, we compared the total number of spots
209 per cell in the case of SaFtsZ and EcFtsZ from treated and untreated cells. For statistical
210 analysis, we used both estimation statistics (effect size and 95 % CI) and significance
211 testing by null hypothesis statistical tests (Claridge-Chang and Assam 2016). When
212 treated with sanguinarine, a reduction in the number of spots per cell was observed in both
213 SaFtsZ and EcFtsZ, with an effect size of -4.82 [95% CI -5.7, -3.9] and -5.4 [95% CI -9.7, -
214 1.1] respectively **(Fig. 2E i and ii)**. Similarly, the addition of berberine also exhibited a
215 similar reduction in the number of spots per cell in both SaFtsZ and EcFtsZ, with an effect
216 size of -5.6 [95% CI -7.9, -3.3] and -12.4 [95% CI -19.5, -5.4] respectively **(Fig. 2G i and**
217 **ii)**. Since HpFtsZ assembled into filaments, we compared the total length of the polymer
218 per cell in the presence or absence of the drugs. Both sanguinarine and berberine
219 resulted in a significant reduction of total polymer length per cell with an effect size of -45.3
220 [95% CI -60, -30] and -92 [95% CI -151, -33.5], respectively **(Fig. 2 E iii and G iii)**.

221 In addition, we also quantified density, which is a measure of assembled
222 cytoskeleton per unit area in a given cell (Henty-Ridilla et al. 2014; Higaki 2017). We had
223 recently used density as a measure to successfully quantify assembly defects of an ATP

224 hydrolysis mutant of *Spiroplasma citri* MreB (Pande et al. 2022). Cells expressing SaFtsZ,
225 EcFtsZ or HpFtsZ and treated with the drugs had lower density values as compared to
226 control untreated cells, suggesting an inhibitory effect of the drugs on cytoskeleton
227 assembly. In the case of sanguinarine, the effect sizes were -1.72 [95% CI -2.5, -0.9], -2.6
228 [95% CI -4.5, -0.6] and -1.1 [95% CI -1.5, -0.5] for SaFtsZ, EcFtsZ and HpFtsZ
229 respectively **(Fig. 2E i – iii)**. The effect size in the case of berberine-treated cells were -
230 1.8 [95% CI -2.5, -1.1], -3.4 [95 %CI -5.3, -1.5] and -1.6 [95% CI -2.5, -0.6] for SaFtsZ,
231 EcFtsZ and HpFtsZ respectively **(Fig. 2G i – iii)**. These results suggest that sanguinarine
232 and berberine had an effect on the assembly of FtsZ from all three species, *S. aureus*, *H.*
233 *pylori* and *E. coli* when expressed in fission yeast cells.
234 Although we did not observe any growth defect in yeast cells at lower
235 concentrations of the drugs, earlier studies have suggested that yeast cells possibly
236 require higher concentrations of drugs than used for mammalian cells due to the presence
237 of the cell wall, which is particularly thick in *S. pombe* (Benko et al. 2017; Pérez and Ribas
238 2004). We thus explored the possibility of cell toxicity to yeast cells at higher
239 concentrations of the drugs. At higher concentrations, both sanguinarine (135.95 μM) and
240 berberine (134.45 μM) induced significant morphological defects in yeast cells **(Fig. 2H)**.
241 However, even at higher concentrations, neither of the drugs showed any visible effect on
242 yeast microtubules **(Fig. S3 A and B)**.
243 Further, in order to test if the effects of sanguinarine and berberine were specific to
244 FtsZ polymerization, we tested its activity on the *E. coli* actin homologue
245 MreB. Sanguinarine and berberine showed no effects on MreB assembly **(Fig. S3C iii**
246 **and iv)**. However, A22, a known inhibitor of MreB (Gitai et al. 2005; Iwai et al. 2002), as
247 previously reported (Srinivasan et al. 2007), completely inhibited the polymerization of
248 EcMreB in fission yeast **(Fig. S3C ii)**.
249

250 ***PC190723 induces polymerization of both SaFtsZ and HpFtsZ, but not EcFtsZ***

251 Several studies have shown that PC190723 binds SaFtsZ, and crystal structures
252 have revealed the binding site to be the inter-domain cleft of FtsZ (Haydon et al. 2008;
253 Matsui et al. 2012a; Tan et al. 2012). Further, PC190723 preferentially binds to the T state
254 of SaFtsZ, inhibits the GTPase activity of FtsZ, induces polymerization and stabilizes FtsZ
255 filaments (Andreu et al. 2010; Elsen et al. 2012; Miguel et al. 2015; Fujita et al. 2017). We,
256 therefore, decided to test PC190723 for its effects on SaFtsZ, HpFtsZ and EcFtsZ
257 expressed in fission yeast cells. The effect of PC190723 was tested at various
258 concentrations (ranging from 14.06 μM to 70.27 μM) on the assembly of FtsZ
259 polymers. At 8 – 10 hours after growth in the induction medium (EMM without thiamine),
260 the majority of cells expressing SaFtsZ or HpFtsZ showed only diffuse FtsZ molecules in
261 the cytoplasm and had not yet assembled into structures. Therefore, *S. pombe* cells
262 carrying SaFtsZ or HpFtsZ constructs were grown at 30ºC in the absence of thiamine for 8
263 – 10 hours before DMSO or PC190723 was added to the cultures. PC190723 or DMSO
264 was added to cultures at this point and incubated at 30ºC for further 4 hours. In cultures
265 where DMSO was added, 446 ± 5 (SEM; 500 cells counted for each replicate; N = 3) cells
266 expressing SaFtsZ **(Fig. 3 A and B ii)** and 378 ± 4 (SEM; 500 cells counted for each
267 replicate; N = 3) cells expressing HpFtsZ **(Fig. 3 D and E ii)** were found to have only
268 diffuse FtsZ molecules in the cytoplasm.

269 On the contrary, cultures treated with PC190723 (35 μM or more) had a significantly
270 more proportion of cells with FtsZ assembled into polymers as compared to untreated cells
271 (DMSO) for SaFtsZ **(Fig. 3 A and B iv)** and HpFtsZ **(Fig. 3 D and E iv)**. PC190723 did
272 not alter the assembly of SaFtsZ into ring-like structures or HpFtsZ into spiral filaments
273 **(Fig. 3 C and F; Fig. S2)**. Further, with an increasing concentration of PC190723, there
274 was a concomitant increase in the proportion of cells that contained polymerized FtsZ in
275 the case of SaFtsZ **(Fig. 3A)** and HpFtsZ **(Fig. 3C)**. Quantification of the number of spots

276 per cell showed an increase in the number of SaFtsZ spots in the presence of PC190723
277 with an effect size of 5.8 [95%CI 3.5, 8.1] (cells counted for each replicate was ≥ 18 and ≤
278 85; N = 4). Moreover, the amount of assembled cytoskeleton per unit area in a cell also
279 increased, with an effect size of 2.6 [95%CI 1.7, 3.6] (cells counted for each replicate was
280 ≥ 86 and ≤ 176; N = 4), when treated with PC190723 **(Fig. 3G)**. Similarly, in the case of
281 HpFtsZ, the total length of the polymer per cell and density were higher in the presence of
282 PC190723. The effect size for polymer length and density were 80.3 [95%CI 10.4, 150.2]
283 and 1.9 [95%CI 0.14, 3.7] (cells counted for each replicate was ≥ 104 and ≤ 159; N = 4),
284 respectively **(Fig. 3H)**. However, no such difference was observed in the absence or
285 presence of PC190723 in cells expressing EcFtsZ **(Fig. 3 I and J)** and is consistent with a
286 recent study that concluded that the inhibitory activity of PC190723 on *E. coli* was
287 independent of FtsZ (Khare et al. 2019). These observations suggested that PC190723
288 resulted in an early assembly of FtsZ into polymers in the case of SaFtsZ and HpFtsZ, but
289 it did not have any effect on EcFtsZ. Further, the addition of PC190723 after the
290 appearance of FtsZ polymers in yeast cells did not have any notable effect on the FtsZ
291 structures **(Fig. S4)**. Our results presented here thus support the earlier reports that
292 PC190723 acts to reduce the critical concentration of FtsZ polymerization of SaFtsZ
293 (Andreu et al. 2010; Elsen et al. 2012).
294 Earlier studies had reported that PC190723 was non-toxic to eukaryotic cells,
295 including budding yeast (Haydon et al. 2008). We further tested if PC190723 resulted in
296 morphological defects in *S. pombe*, like sanguinarine and berberine, at higher
297 concentrations. However, consistent with the earlier reports, PC190723 was inactive
298 against *S. pombe* at both 56.2 μM and 140.6 μM and did not cause any morphological
299 changes **(Fig. 2H iv)**. Further, PC190723 did not disrupt the yeast microtubules at either
300 of the concentrations **(Fig. S3 A iv and B iv)**.
301

302 ***PC190723 stabilizes polymers and slows down the turnover rates of both SaFtsZ***
303 ***and HpFtsZ***

304 We tested if PC190723 impacted the turnover rates of SaFtsZ and HpFtsZ using
305 fluorescence recovery after photobleaching (FRAP) experiments. Fluorescence recovery
306 was measured after bleaching a complete SaFtsZ spot or patch either in untreated cells
307 **(Fig. 4A)** or in cells treated with 56.2 μM of PC190723 **(Fig. 4B)**. Representative graphs
308 showing the fluorescence recovery of SaFtsZ in the absence of PC190723 or the presence
309 of 56.2 μM of PC190723 are depicted in **Figure 4C** and **Figure 4D,** respectively, and the
310 plots for all such cells are shown **(Fig. S5 A and B)**. While SaFtsZ exhibited rapid
311 dynamics with a half-time ($t_{1/2}$) of 3.61 ± 0.41 seconds (95% CI; N = 10) in the absence of
312 PC190723, the half-time ($t_{1/2}$) of fluorescence recovery increased by nearly 3-fold to 11.34
313 ± 3.52 seconds (95% CI; N = 10) in the presence of PC190723 **(Fig. 4E)**, giving an effect
314 size of 7.7 [95% CI 4.0, 11.5]. Fluorescence recovery of HpFtsZ was similarly measured
315 after bleaching a small part of HpFtsZ filaments in both untreated cells **(Fig. 4F)** or in cells
316 treated with 56.2 μM of PC190723 **(Fig. 4G)**. Representative graphs of the fluorescence
317 recovery of HpFtsZ in the absence of PC190723 or the presence of 56.2 μM of PC190723
318 are shown in **Figure 4H** and **Figure 4I,** respectively. The plots for all such cells are shown
319 **(Fig. S5 C and D).** The effect of PC190723 on the turnover rates of HpFtsZ was milder
320 but significant and resulted in 1.96 times fold change in the fluorescence recovery half-
321 time ($t_{1/2}$) rates with an effect size of 5.9 [95% CI 3.5, 8.3]. The recovery half-time ($t_{1/2}$)
322 was 6.16 ± 0.89 seconds (95% CI; N = 10) in untreated cells and is consistent with the
323 earlier reports (Specht et al. 2013). In the presence of PC190723, it increased to 12.06 ±
324 2.14 seconds (95% CI; N = 10) **(Fig. 4J)**. Interestingly, compound 8j, a related benzamide
325 derivative, has been shown to slow down FtsZ-ring turnover by 3-fold in *B. subtilis* (Adams
326 et al. 2011). These results from the FRAP studies show that PC190723 affects the

327 dynamics and turnover of both *S. aureus* and *H. pylori* FtsZ filaments, consistent with an
328 effect of stabilization of filaments by the inhibitor.
329
330 ***SaFtsZ$^{G196A}$ and HpFtsZ$^{G213A}$ expressed in yeast exhibit PC190723 resistance***
331 A comparison of the FtsZ sequences from various bacterial species that were
332 tested for growth inhibition by PC190723 had revealed several key residues in FtsZ,
333 determining its susceptibility or resistance (Haydon et al. 2008). In both *B. subtilis* and *S.*
334 *aureus*, a single point mutation in FtsZ at G196 position to alanine (A) has been shown to
335 result in a several-fold increase in the minimal inhibitory concentration of PC190723
336 (Stokes et al. 2013). Therefore, we next tested if we could experimentally observe
337 resistance to PC190723 by FtsZ mutants G196A in our yeast expression
338 system. Structure-based sequence alignment and comparisons showed that the
339 equivalent residue of G196 in HpFtsZ is G213 and is conserved across the FtsZs **(Fig.**
340 **S6)**. Hence we changed G213 in HpFtsZ to alanine (Ala) and expressed HpFtsZ$^{G213A}$ in
341 fission yeast. We then tested the effect of PC190723 on the mutation in a similar manner
342 as described above, at a point when untreated cells predominantly exhibited diffuse
343 fluorescence or short polymers.
344 In the case of HpFtsZ$^{G213A}$, we found that only 41 ± 2.9 % (95% CI; N = 3; 500 cells
345 were counted for each replicate) of the cells treated with 56.2 μM PC190723 as compared
346 to 31 ± 16.4 % (95% CI; N = 3; 500 cells were counted for each replicate) in untreated
347 cells had FtsZ polymers **(Fig. 5 A – C)**. As compared to the effect size of 28.2 [95% CI
348 19.8, 36.7] for HpFtsZ$^{WT}$, the effect size for HpFtsZ$^{G213A}$ treated with PC190723 was 10.4
349 [95% CI -1.1, 21.9] with a negative value for the lower bound. Thus, there was no
350 significant increase in the number of cells having FtsZ polymers in the mutant HpFtsZ$^{G213A}$
351 upon treatment with PC190723 **(Fig. 5A)**. In comparison, as described above, HpFtsZ$^{WT}$
352 exhibited a significant increase in the number of cells having FtsZ polymers (70% of cells)

353 when treated with PC190723 (**Fig. 5A and 5C**). Although PC190723 did not have an
354 effect on the G213A mutant of HpFtsZ, HpFtsZ$^{G213A}$ was proficient in polymerization and
355 assembled into filaments **(Fig. S7A)**.
356 We also expressed SaFtsZ$^{G196A}$ in fission yeast cells from the same *nmt41/42*
357 promoter as for the wild-type SaFtsZ. Surprisingly, unlike HpFtsZ$^{G213A}$, we found that
358 SaFtsZ$^{G196A}$ failed to assemble into any structures in yeast cells **(Fig. S7B ii)**. Although it
359 has been shown that FtsZ$^{G196A}$ is functional for cell division in both *S. aureus* and *B.*
360 *subtilis* and forms Z-rings in the latter (Haydon et al. 2008; Stokes et al. 2013; Adams et al.
361 2016), mutations at G196 is also known to result in growth defects in *S. aureus* (Stokes et
362 al. 2013; Adams et al. 2016). Nonetheless, the addition of 56.2 μM of PC190723 also did
363 not induce any polymerization or the assembly of SaFtsZ$^{G196A}$ **(Fig. S7B iv)**. Taken
364 together, our results show that mutations that render FtsZ insensitive to PC190723 do not
365 assemble early into polymeric structures in the presence of the drug, suggesting that
366 PC190723 fails to bind SaFtsZ$^{G196A}$ and HpFtsZ$^{G213A}$.
367
368 ***PC190723 docks into the inter-domain cleft of the HpFtsZ* modelled structure *in the***
369 ***T state***
370 Crystal structures of SaFtsZ bound to PC190723 **(Fig. 6A and B;** PDB ID 4DXD**)** reveal
371 the binding mode of PC190723 to the T state conformation of the protein (Matsui et al.
372 2012b; Tan et al. 2012). In the T state conformation of FtsZ, the cleft between the H7 helix
373 and CTD is opened, and hence the inhibitor can be accommodated in the pocket. The
374 residues Gly196, Leu200, Val203, Asn208, Leu209, Met226, Ile228, Asn263, Val297,
375 Thr309 and Ile311 interact with the inhibitor in SaFtsZ **(Fig. 6A)**. In the R state
376 conformation of FtsZ, the inter-domain cleft is closed and hence does not have an
377 adequate gap between the H7 helix and the central beta-sheet of CTD (S7, S8, S9, S10
378 strands) to accommodate PC190723 into the cleft. The inhibitor shows clashes with

379 residues of the cleft when the T state structure (PDB ID: 4DXD) is superimposed with the
380 R state structure (PDB ID: 5H5I) of SaFtsZ **(Fig. 6B)**. A structure-based multiple
381 sequence alignment reveals that many of the residues in FtsZ involved in the interaction
382 with PC190723 are conserved in HpFtsZ **(Fig. S6 A and B)**.

383 We further resorted to *in silico* approaches to determine if the inter-domain cleft in
384 HpFtsZ could accommodate PC190723. We thus modelled HpFtsZ using SwissModeller
385 (Waterhouse et al. 2018) with the T state of SaFtsZ as a template and superposed it with
386 the PC190723 bound SaFtsZ structure (4DXD) to see whether PC190723 can fit into the
387 modelled HpFtsZ structure **(Fig. 6C)**. Analysis of PC190723 in the inter-domain cleft of
388 the HpFtsZ model indicated that several residues that made direct contact with the drug in
389 the crystal structure of the PC190723-SaFtsZ complex (4DXD) were conserved in HpFtsZ
390 and shown to be within interacting distances of PC190723. Phe281 of HpFtsZ could
391 potentially interact by a stacking interaction with the ring of PC190723. The side chain of
392 Thr328 is at a distance capable of forming hydrogen bonds, while the side chain of Ile217
393 forms van der Waals interaction with the inhibitor **(Fig. 6C and Fig. S6B)**. Unlike in the R
394 state, the residues in the S7, S8, S9 and S10 beta-sheets or the H7 helix do not clash with
395 the inhibitor in the T state.

396

397 ***Resistance to PC190723 is mediated by salt-bridge interactions that prevent drug***
398 ***binding in the inter-domain cleft.***

399 A single point mutation in FtsZ at position Gly196 in *B. subtilis* and *S. aureus* is
400 sufficient to render them resistant to PC190723. However, it was also noted that while the
401 susceptible species were characterized by the presence of valine (Val) at position 307,
402 some other species of bacteria that were naturally resistant to PC190723 contained
403 arginine (Arg) or histidine (His) at this position (Haydon et al. 2008; Kaul et al.

404 2013b). Surprisingly, HpFtsZ contains an arginine at this position (Arg326), and yet our
405 results from the yeast expression studies suggested that PC190723 had an effect on the
406 polymerization and dynamics of HpFtsZ. In order to further probe this apparent
407 discrepancy, we analyzed the sequences and molecular structures of FtsZ from various
408 species that included both susceptible and resistant species **(Fig. S6A)**. A detailed
409 structure-based sequence analysis of FtsZ showed that in species that are resistant to
410 PC190723, there are possibly two salt bridges that might play an important role in
411 occluding the inter-domain cleft **(Fig. 6D and Fig. S6)**. The blockage of this cleft might
412 prevent the binding of the inhibitor **(Fig. 6D)**. In species like *E. coli* that are resistant to
413 PC190723, these blockages constitute two salt bridge interactions- Arg307 and Glu198
414 (shown in red); Asp299 and Arg202 (shown in violet) and one hydrogen bond interaction
415 between the OH group of Ser227 and the main chain of Gly191 (shown in brown) **(Fig.
416 6D)**. These interactions are absent in *S. aureus* FtsZ; thereby, the inhibitor can be
417 accommodated in the cleft. However, in HpFtsZ, the equivalent position of Glu198 in
418 EcFtsZ is threonine (Thr216), which is smaller than glutamic acid (Glu) and probably far off
419 to engage in any interaction with Arg326 (the equivalent of Arg307 in EcFtsZ) **(Fig. 6E)**.
420 Thus, the salt bridge which might block the inhibitor from binding at the cleft is not present
421 in HpFtsZ **(Fig. 6E)**, thereby possibly allowing PC190723 to bind.
422 Therefore, restoring the salt-bridge interactions between the amino acids at
423 positions 326 and 216 in HpFtsZ should render it insensitive to PC190723. In order to test
424 this hypothesis, we changed Thr216 in HpFtsZ to glutamic acid (Glu), expressed the
425 mutant HpFtsZ$^{T216E}$ in fission yeast and tested the effect of PC190723 on this mutation. In
426 accordance with the structural analysis, we found no significant difference in the number of
427 cells having FtsZ polymers in the mutant HpFtsZ$^{T216E}$ upon treatment with PC190723 **(Fig.
428 5 A and D)**. In the presence or absence of PC190723, HpFtsZ$^{T216E}$ expressing cells
429 showed 47 ± 3.4 % (95% CI; N = 3; 500 cells were counted for each replicate) and 48 ±

430 14.8 % (95% CI; N = 3; 500 cells were counted for each replicate) respectively, that
431 assembled FtsZ polymers **(Fig. 5A)**. This was unlike HpFtsZ$^{WT}$ **(Fig. 5A and 3D),** where
432 almost 70 % of the cells treated with PC190723 contained polymers as compared to a
433 mere 38 % in untreated cells **(Fig. 5A and 3D)**. The effect size for HpFtsZ$^{WT}$ treated with
434 PC190723 was 28.2 [95% CI 19.8, 36.7] as compared to the effect size for HpFtsZ$^{T216E}$
435 treated with PC190723, which was 0.9 [95% CI -9.6, 11.5] with a negative value for the
436 lower bound of the confidence interval. Further, like HpFtsZ$^{G213A}$, HpFtsZ$^{T216E}$ was
437 capable of polymerization and assembled into polymers upon expression in fission yeast
438 **(Fig. S7C)**. Our results here, therefore, suggest that the salt-bridge interactions between
439 residues in the H7 helix and adjacent sheets (S9 and S10) in the inter-domain cleft form
440 the basis for the inability of FtsZ in many species to bind to PC190723 rather than a single
441 residue (Arg or His) at position 307 (EcFtsZ).
442

443 **Discussion**

444 In this study, we have attempted to develop a cell-based assay using fission yeast
445 (*S. pombe*) as a heterologous expression host, which would enable the screening of
446 compounds that could directly affect FtsZ polymerization as well as identify potential
447 toxicity to yeast (or eukaryotic) cells simultaneously. As a proof-of-principle, we first
448 assessed the ability of FtsZ from two pathogenic species, *S. aureus* and *H. pylori,* to
449 assemble into structures in fission yeast and tested the effects of known FtsZ modulators,
450 sanguinarine, berberine and PC190723 on these FtsZ assemblies. We show that both
451 SaFtsZ and HpFtsZ assembled into structures in fission yeast. While SaFtsZ assembled
452 into spots/ patches or ring-like structures, HpFtsZ assembled into both linear and spiral
453 polymers. Interestingly, spiral filaments of FtsZ polymers of *H. pylori* have also been
454 reported in bacterial cells and when expressed in *Drosophila melanogaster* S2 Schneider
455 cells (Specht et al. 2013), suggesting that assembly into helical filaments might be intrinsic

456 to HpFtsZ polymers. Previous studies have shown that various factors such as molecular
457 crowding, variable C-terminal regions and bound nucleotide state lead to the formation of
458 supramolecular structures like twisted helical structures, toroids and rings similar to those
459 that have been observed *in vivo* (Popp et al. 2009; Huecas et al. 2017). Thus, the
460 molecular crowding due to the dense cytoplasm of the yeast cells could have possibly
461 induced the spiral and ring-like assembly of FtsZ polymers (Erickson et al. 2010).

462 Several approaches have been used to screen small molecules targeting bacterial
463 cell division and FtsZ. While *in vitro* methods such as NMR (Domadia et al. 2007; Sun et
464 al. 2014; Araújo-Bazán et al. 2019) and crystallography (Läppchen et al. 2008; Fujita et al.
465 2017) are valuable and offer information on distinct binding sites, these are not efficient for
466 screening. Electron microscopic examination can distinguish the effects of the compounds
467 being tested on the FtsZ protofilament assembly and lateral associations (Nova et al.
468 2007; Kaul et al. 2012; Anderson et al. 2012; Sun et al. 2014; Huecas et al. 2017; Kumar et
469 al. 2011; Park et al. 2014). Other techniques that are routinely used include fluorescence
470 anisotropy (Ruiz-Avila et al. 2013; Park et al. 2014), 90º light-scattering assay (Mukherjee
471 and Lutkenhaus 1999) and dynamic light scattering (Hou et al. 2012; Di Somma et al.
472 2020) for assessing inhibition of FtsZ assembly (Irwin et al. 2015; Lui et al. 2019; Kaul et al.
473 2012; Nova et al. 2007; Anderson et al. 2012). Other easily scalable high-throughput
474 assays include FCS/FCCS and FRET-based methods (Hernández-Rocamora et al. 2015;
475 Mikuni et al. 2015; Reija et al. 2011).

476 *In vivo* assays relying on cell filamentation phenotype coupled with the localization
477 of Z-ring might be a good indicator of FtsZ being the direct target. However, since bacteria
478 can undergo cell filamentation and not assemble FtsZ rings in response to a variety of
479 conditions, including DNA damage (Mukherjee et al. 1998) and disruption of membrane
480 potential (Strahl and Hamoen 2010), the *in vivo* assay is not so useful unless combined

481 with the *in vitro* assays mentioned above. Finally, the isolation of resistance mutants in
482 FtsZ to the drug can provide strong evidence of FtsZ being the direct target.
483 Reconstitution systems are powerful and provide excellent control over the system,
484 but they are emerging technologies and are technically challenging. Reconstitution
485 systems include a variety of methods, such as the use of membrane nanodiscs,
486 microbeads of different materials, supported bi-layer membranes (SLBs) and biomimetic
487 systems that provide cell-like environments (Monterroso et al. 2013; Rivas et al. 2014).
488 While *in vitro* biochemical assays and reconstitution systems are useful to find molecules
489 that directly target FtsZ, they are cumbersome and need to be performed at optimal
490 physiological pH and ionic conditions, which can be considerably variable among FtsZ
491 from different species.
492 Our results on the ability of sanguinarine and berberine to specifically affect the
493 assembly of FtsZ and not MreB in fission yeast highlight the utility of the heterologous
494 expression system as a platform to identify molecules that specifically affect FtsZ
495 polymerization. The yeast platform offers a cellular context mimicking the cytoplasm for
496 cytoskeletal assembly. The system is simple to replicate in any laboratory, including those
497 focused on chemical synthesis with minimum microbiological expertise and can be easily
498 reproduced and scaled up as well. However, one of the major disadvantages of using
499 fission yeast could be the need to use much higher concentrations of drugs than normally
500 used for mammalian cell cultures to achieve an inhibitory effect. This could probably be
501 due to the poor permeability of certain drugs in fission yeast because of its thick cell wall
502 (Benko et al. 2017; Pérez and Ribas 2004). A similar effect of toxicity might arise at much
503 lower concentrations in other eukaryotic cells, such as human cells. Consistently, while
504 sanguinarine and berberine are known to affect the eukaryotic microtubules at 10 μM – 20
505 μM concentrations (Lopus and Panda 2006; Wang et al. 2016; Raghav et al. 2017),
506 morphological effects on yeast cells were observed only at concentrations > 100 μM.

507 However, yeast microtubules were not affected by berberine and sanguinarine.
508 Differences in membrane lipid profiles and MDR efflux pumps between yeasts and
509 mammalian cells might also contribute to differential resistance to the drugs being tested
510 (Balzi and Goffeau 1991). Conversely, an inhibitory effect in yeast cells may not
511 necessarily translate into toxicity in a human cell. These and the permeability of drugs in
512 yeast cells represent an important caveat in using such heterologous expression systems
513 for the screening of compounds against target molecules. However, notwithstanding this
514 caveat, the heterologous system provides significant advantages in assessing the direct
515 effects of the drug on FtsZ assembly. Moreover, fission yeast-based high-throughput
516 platform screening methods using imaging have been successfully adapted to the
517 screening of drugs against HIV-1 proteases by large-scale screening facilities such as the
518 NIH Molecular Libraries Probe Production Centers Network in the Molecular Libraries
519 Program, leading to several candidate drugs (Benko et al. 2017, 2019). This aspect also
520 emphasizes the benefit of utilizing an economic eukaryotic heterologous host for testing
521 drugs targeting bacterial proteins. Any compound that potentially affects eukaryotic
522 function can be easily identified and discarded at the screening step, thus reducing time
523 and costs on further pharmacological analysis in the drug development pipeline.
524 PC190723 has been one of the most promising drugs against FtsZ and remains the
525 only inhibitor for which the binding site in FtsZ has been clearly established. However,
526 PC190723 predominantly affects Gram-positive bacteria and FtsZ from Gram-negative
527 bacteria have been shown or predicted to be resistant (Haydon et al. 2008). Several
528 efforts have been made to target Gram-negative bacteria with derivatives of benzamide.
529 Examples include difluorobenzamides, substituted benzodioxanes, heterocyclic and non-
530 heterocyclic derivatives (Straniero et al. 2017; Chai et al. 2020; Straniero et al. 2020a,
531 2020b). Although many exhibited promising activity *in vitro*, most were substrates for the
532 AcrAB class of efflux pumps (Chai et al. 2020; Kaul et al. 2014; Straniero et al. 2020a,

533 2020b; Casiraghi et al. 2020). Thus, the poor membrane permeability, signature outer
534 membrane, particularly lipopolysaccharide (LPS) structure (Wang et al. 2021), the
535 presence of multiple efflux pumps in species such as *E. coli*, *Klebsiella pneumonia* and
536 *Pseudomonas aeruginosa* (Piddock 2006), and differences in FtsZ sequences in the
537 binding-site (Kaul et al. 2013b; Miguel et al. 2015) have been cited as reasons for lack of
538 susceptibility of Gram-negative bacteria to benzamide derivatives (Casiraghi et al. 2020).
539 More recently, two molecules, TXA6101 and TXY6129, with substituted 2,6-
540 difluorobenzamide scaffold, have been shown to inhibit the polymerization of both *E. coli*
541 and *Klebsiella pneumoniae* FtsZ. Moreover, despite being substrates for efflux pumps,
542 TXA6101 induced morphological changes in *K. pneumoniae* (Rosado-Lugo et al. 2022).
543 Studies in the past on the effects of PC190723 on *E. coli* have been confusing, with a few
544 reports suggesting an effect on FtsZ polymerization resulting in cell filamentation (Kaul et
545 al. 2014), while others did not find any effect on EcFtsZ (Andreu et al. 2010; Anderson et
546 al. 2012; Khare et al. 2019). The outer membrane has been shown to be a permeability
547 barrier for PC190723 in *E. coli* (Khare et al. 2019; Chai et al. 2020). In addition, the
548 Resistance-Nodulation-Division (RND) family of efflux pumps has been attributed to
549 resistance against 2,6-difluorobenzamide derivatives, including TX436 (a prodrug of
550 PC190723) in Gram-negative bacteria (Kaul et al. 2014).
551 It was, therefore, of interest to test the effects of PC190723 on FtsZ assembly in the
552 yeast expression system, wherein the interpretations are not affected by the compounding
553 factors such as differential membrane permeability or efflux pumps. Our assay provides
554 for a direct comparison of the effect of PC190723 on FtsZ from different species. While
555 our results presented here clearly suggest that PC190723 does not affect the assembly of
556 EcFtsZ, it exerted an effect on HpFtsZ, which is also from a Gram-negative bacterium.
557 Assemblies of SaFtsZ and HpFtsZ structures appeared in fission yeast cells at a much
558 earlier time when treated with PC190723, suggesting that the drug acted to lower the

559 critical concentration of FtsZ polymerization. Further, FRAP experiments performed on
560 SaFtsZ and HpFtsZ suggest that PC190723 affects the dynamics of FtsZ polymers and
561 slows down the turnover rates. We had earlier shown that FtsZ mutants defective in GTP
562 hydrolysis expressed in fission yeast have slower turnover rates, as measured by
563 fluorescence recovery half-times ($t_{1/2}$) rates (Srinivasan et al. 2008).- These results are
564 also consistent with the earlier findings that PC190723 acts to induce FtsZ polymerization
565 and stabilize FtsZ filaments (Andreu et al. 2010; Elsen et al. 2012; Miguel et al. 2015; Fujita
566 et al. 2017) and its derivative compound, 8j acting to slow down FtsZ-ring turnover by 3-
567 fold in *B. subtilis* (Adams et al. 2011).
568
569 Finally, our studies here suggest that resistance to PC190723 in FtsZ from Gram-
570 negative bacteria like *E. coli* is a result of occluding salt-bridge interactions in the inter-
571 domain cleft between the H7 helix and adjacent sheets (S9 and S10) and may not be due
572 to a single residue (Arg or His) at position 307. Although HpFtsZ contains an arginine at
573 the equivalent position (Arg326), this residue cannot engage in a salt bridge since HpFtsZ
574 has a threonine (Thr) at position 216 (the equivalent of Glu198 in EcFtsZ). Restoring the
575 salt-bridge interaction in HpFtsZ by changing Thr216 to glutamate (E) conferred resistance
576 to PC190723 in our yeast expression studies. However, PC190723 failed to exert growth
577 inhibition of *H. pylori,* probably owing to outer membrane permeability barriers. Thus,
578 although further genetic, cell biological and biochemical studies will be required to fully
579 elucidate the resistance of *H. pylori* cells to PC190723, our studies here provide new
580 insights into the molecular determinants in FtsZ that lead to resistance against PC190723.
581 A powerful emerging technique based on cytological profiling has been successfully used
582 to identify the cellular pathways targeted by the inhibitors (Nonejuie et al. 2013; Martin et
583 al. 2020), including cell division inhibition by FtsZ (Araújo-Bazán et al. 2016). The recent
584 advances in computational image analysis and deep learning approaches (von Chamier et

585 al. 2021; Spahn et al. 2022) could further advance image-based screening for FtsZ
586 inhibitors (Andreu et al. 2022). Thus, our results here suggest that the fission yeast
587 expression system can be used to identify small molecules that directly target FtsZ, probe
588 the molecular determinants of resistance and establish a proof-of-concept of an *in vivo*
589 cell-based assay to discover antimicrobials that specifically target the bacterial
590 cytoskeleton.
591

592 **MATERIALS AND METHODS:**

593 **Growth and culture of bacteria and yeast:**

594 The strains and plasmids used in this study are listed in **Supplementary Table S1**. *E. coli*
595 strains and *S. aureus* (ATCC 25923) were grown in LB medium at 37°C, whereas *H. pylori*
596 (strain *H. pylori* 26695) was grown in Brucella broth with 10 % fetal bovine serum media at
597 37°C with 10 % $CO_2$. *E. coli* cultures carrying plasmids were grown in LB medium
598 containing appropriate antibiotics (carbenicillin at 100 µg/ mL; kanamycin at 50 µg/ mL;
599 chloramphenicol at 34 µg/ mL). *S. pombe* strain 192 (*h− leu1-32 ura4-D18*) and mCherry-
600 Atb2 strains were grown at 30°C in YES medium. Transformation of *S. pombe* was carried
601 out using the Lithium acetate method as described previously (Bähler et al. 1998) and
602 plated on selective Edinburg minimal medium (EMM) plates containing 15 µM thiamine.
603 EMM plates and broth were supplemented with adenine (0.225 mg/ mL of media), histidine
604 (0.225 mg/ mL) and leucine (0.225 mg/ mL) or uracil (0.1125 mg/ mL) as
605 necessary. Thiamine was used at a final concentration of 15 µM on the agar plates to
606 repress expression from the medium-strength pREP41/42 plasmids. All experiments were
607 done with *S. pombe* growing at 30°C in exponential phase ($OD_{600}$ of 0.3 – 0.6) and were
608 maintained thus by intermittent dilution of cultures. Inhibitors PC190723, sanguinarine,
609 berberine and A22 were dissolved in DMSO and added to *S. pombe* cultures at final
610 concentrations as indicated in the text or figure legends.

611

612 **Plasmids and constructs:**

613 *Cloning of EcFtsZ, HpFtsZ & SaFtsZ into yeast expression vector pREP42:*

614 EcFtsZ, SaFtsZ and HpFtsZ refer to FtsZ from *E. coli*, *S. aureus* and *H. pylori*,
615 respectively. The cloning of EcFtsZ-GFP (pCCD4) into pREP42 has been described
616 previously (Srinivasan et al. 2008). Genomic DNA was isolated from *H. pylori* and *S.*
617 *aureus* wild-type strains using the Genomic DNA Isolation kit. These genomic DNA were
618 used as a template in a PCR reaction using high-fidelity Q5 polymerase to amplify the *ftsZ*
619 genes of these bacteria. The plasmids pCCD712 and pCCD713 expressing *H. pylori* FtsZ-
620 GFP (HpFtsZ-GFP) and *S. aureus* FtsZ-GFP (SaFtsZ-GFP), respectively, were
621 constructed by cloning the amplified PCR product into pCCD51 using restriction-free (RF)
622 cloning method (van den Ent and Löwe 2006). pCCD51 was constructed as follows: GFP
623 was amplified by PCR from pCCD4 using oligonucleotides RSO73 and RSO74. The PCR
624 product was subsequently digested with SmaI and ligated into pREP42 (Moreno et al.
625 2000), linearized with the same enzyme. Site-directed mutagenesis was carried out
626 following the Stratagene™ Quickchange-II site-directed mutagenesis procedure using
627 high-fidelity Q5 polymerase. The oligonucleotides used are listed in **Supplementary**
628 **Table S2,** and the list of chemical reagents with their catalogue numbers is listed in
629 **Supplementary Table S3**.

630

631 **Microscopy and Fluorescence Recovery after Photobleaching:**

632 For imaging, the cells were mounted onto 1.7% or 2% agarose pads containing media in
633 cavity slides and covered with a coverslip No. 1.5 prior to sealing with VALAP (1:1:1
634 mixture of vaseline, lanolin and paraffin). Images were acquired using an epifluorescence
635 microscope (DeltaVision™ Elite) with a 100 X oil immersion objective lens of NA 1.4 and
636 equipped with a Photometrics CoolSNAP™ HQ2 camera. An oil with a refractive index of

637 1.516 was used for imaging yeasts. Excitation filters and emission filters of 475/28 nm and
638 525/48 nm were used to image GFP. Z-stacks were acquired with a Z-depth of 0.2 or 0.3
639 µm. SoftWorX™ software was used to perform deconvolution using the iterative-
640 constrained algorithm (Agard 1984) with the number of cycles set to 10 (ten). 3D-SIM on
641 *S. pombe* was performed as described previously (Pande et al. 2022). Cells were
642 mounted on an agarose pad as described above and imaged using a DeltaVision OMX-SR
643 Blaze microscope. Raw images were acquired using a 60×, NA 1.42 oil-immersion
644 objective lens and a PCO Edge 4.2 sCMOS camera. An exposure time of 2 – 5 ms was
645 used to acquire each image, and Z-stacks were obtained at a step size of 0.125 µm to
646 cover the width of *S. pombe* cells. 3D-SIM were reconstructed using the SI reconstruction
647 module of SoftWorx™ software. FRAP experiments were carried out essentially as
648 described before (Recovery half-times were calculated as described previously (Anderson
649 et al. 2004; Srinivasan et al. 2008) except that a DeltaVision™ equipped with a
650 Quantitative laser module (QLM; X4 Laser) was used for imaging. Photobleaching was
651 carried out using 80% laser power with an argon laser (488 nm) with a pulse time of 0.05
652 sec. Images were acquired before and after photobleaching, and Z-stack images were
653 acquired at fixed intervals with a Z-depth of 0.2 or 0.3 µm. Time-lapse intervals were
654 varied or were typically 1 – 2 seconds apart and acquired for over 2 minutes. Integrated
655 fluorescence intensities in the pre-bleached images and at each time point in the bleached
656 and other regions were measured in Fiji (v 2.0.0-rc-69/1.52p). FRAP experiments were
657 performed on different days, and data were pooled for analysis. All values were exported
658 to Excel (Microsoft™) for further analysis. The recovery half-time ($t_{1/2}$) values mentioned in
659 the text were obtained by fitting the fluorescence recovery curves to a single exponential
660 curve $F(t)= C(1 - e^{-kt})$ and calculated from $t_{1/2} = \ln(2)/k$. The solver function in Excel was
661 used for the least-squares fit of the corrected fluorescence intensities over time to the

662 single exponential equation. All images were processed using Fiji (v 2.0.0-rc-69/1.52p)
663 (Schindelin et al. 2012).

664

665 **Quantitation of the number of spots, polymer length and density**

666 Cells were processed as described above for imaging, and images were acquired as
667 described previously (Pande et al. 2022) for the calculation of the number of spots,
668 polymer length and density. Briefly, imaging was carried out with constant parameters
669 such as fixed illumination of 2% transmission (ND filter), exposure of 0.25 s, binning (1 x 1)
670 and camera gain of 0.5 x). Both differential interference contrast (DIC) and fluorescence
671 channels were imaged, and cell outlines were marked using the freehand drawing tool in
672 Fiji (Schindelin et al. 2012). The cell outlines were saved as regions of interest using the
673 ROI manager. Masking of areas outside of the cell outlines was carried out as described
674 (Higaki 2017) and filled with black colour. The Number of spots per cell was then
675 measured using the OPS threshold IJ1 analyze macro, which is available as a built-in
676 feature in Fiji (v2.0.0-rc-69/1.52p; Schindelin et al. 2012). The macro utilizes a convolve
677 filter with a 5 x 5 kernel and the 'otsu' method for auto-thresholding. A convex hull is used
678 to create the masks of segmented particles, following which the 'analyze particles' plugin is
679 run by the macro. For measuring polymer length and density (amount of cytoskeleton per
680 unit area in a cell), images were processed with the inclusion of masking and
681 skeletonization steps as previously described (Higaki 2017; Henty-Ridilla et al. 2014).
682 Skeletonization was carried out by applying the lpx 2Dfilter in the lpx plugin (Higaki 2017).
683 The specific parameter values giwsIter, mdnmsLen, pickup, aboveThr, shaveLen, delLen,
684 draw, and preGauss were fixed as 5, 15, otsu, default, 5, 5, orgInt and -1, respectively, in
685 the linemode under LineExtract. The LineFeature outputs the measure of the number of
686 pixels with intensities (nPix) after skeletonization and the total polymer length within the
687 selected ROIs. Density, the amount of cytoskeleton assembled per unit area in a cell, is

688 then calculated as nPix divided by the area of the cell. The area of the cell is obtained
689 using the measurement tool in the ROI manager from Fiji.
690

691 **Sequence and structural analysis for PC190723 binding to FtsZ**

692 The sequences of FtsZs from various organisms were taken from UniProt, aligned using
693 Clustal Omega (Sievers et al. 2011), and represented using Jalview (Waterhouse et al.
694 2009). The reference structure taken for the analysis was the previously reported T state
695 structure of SaFtsZ bound to PC190723 (PDB ID: 4DXD), and the residues around 4 Å
696 were determined using UCSF Chimera version 1.13.1 (Pettersen et al. 2004). The
697 residues in SaFtsZ, which contributed to the binding of the inhibitor, were highlighted in the
698 sequence alignment. The reference R state structure (PDB ID: 5H5I) was chosen to see
699 whether the inhibitor can be accommodated in the R state structure of SaFtsZ by
700 superimposing the C- alpha atoms of the nucleotide-binding domain (NBD) of PDB IDs:
701 5H5I and 4DXD. FtsZs from *H. pylori* and *E.coli* were modelled in T state using SWISS-
702 MODEL (Waterhouse et al. 2018), with PDB ID 4DXD as the template. Similarly, the NBD
703 of the modelled structures was superimposed onto the SaFtsZ structure bound to
704 PC190723 and checked whether the inhibitor could be accommodated in the
705 corresponding pocket of the models without significant clashes.
706

707 **Statistical Analysis**

708 All statistical analysis and tests were carried out in Excel (Office 365 or Excel for Mac
709 2011) using the built-in Data Analysis functions or the add-ins XLSTAT or Xrealstat (Real
710 Statistics). A single colony of bacteria or a patch of yeast cells independently grown from
711 freshly streaked out cells on agar plates from frozen glycerol stocks was considered to be
712 a biological replicate (N). A minimum of at least 3 biological replicates was used for every
713 experiment. The dosage effect upon increasing concentrations of PC190723 on FtsZ

714 assembly was assessed using the Cochran-Armitage test. A two-proportions z-test was
715 used for the statistical analysis of the effect of PC190723 on the proportions of cells
716 carrying FtsZ polymers and the calculation of P-values. An unpaired two-sided Student's
717 t-test was used as a statistical test for the FRAP experiments. Statistical tests and P-
718 values are indicated in the figure legends using an asterisk. A P-value ≤ 0.0001, ≤ 0.001,
719 ≤ 0.01, , < 0.05 or ≥ 0.05 indicated by ****, ***, **, * and ns respectively. As an alternative
720 to null-hypothesis significance tests (NHST), we also used estimation statistics to
721 determine the effect size and 95 % confidence intervals (Claridge-Chang and Assam 2016;
722 Ho et al. 2019). Superplots were plotted as described (Lord et al. 2020) using Excel Office
723 365. The error bars plotted are inferential and represent the 95% CI (Cumming et al.
724 2007; Vaux 2014; Pollard et al. 2019).

725

726 **Acknowledgements**

727 The authors are grateful to Prof. Jose Manuel Andreu and Dr. Lidia Araujo-Bazán for their
728 critical reading of the article and valuable comments and suggestions. The authors thank
729 Dr. Asima Bhattacharyya (SBS, NISER, India) for *H. pylori* genomic DNA and Dr. Mithilesh
730 Mishra (DBS, TIFR, Mumbai, India) for strains and plasmids. This work is supported by
731 the Department of Biotechnology (DBT) from BT/PR15183/BRB/10/1443/2015 to RS and
732 BT/PR42977/BRB/10/2022/2021 to RS & GP and DBT Membrane Structural Biology
733 Program grant - BT/PR28833/BRB/10/1705/2018 to PG. PG also acknowledges support
734 from INSPIRE Faculty Fellowship from (IFA12/LSBM-52), Department of Science and
735 Technology, Innovative Young Biotechnologist Award (BT/07/IYBA/2013), Department of
736 Biotechnology (DBT) Membrane Structural Biology Program grant
737 (BT/PR28833/BRB/10/1705/2018), and Science and Engineering Research Board
738 (SERB) Core Research grant (CRG/2018/003795) for infrastructure and staff support.
739 Intramural core funding from the Department of Atomic Energy (DAE) and support staff

740 members at the Centre of Interdisciplinary Sciences, NISER, are acknowledged. We also
741 acknowledge fellowships from DAE to AKS, SMP, BSN, SK, NM and from IISER Pune to
742 JC.

743

744 **Author contributions:**

745 AKS, SMP, BSN, JC and NM conducted the experiments. RS, GP and JC designed and
746 analyzed the work. BSN initiated the work, SMP contributed to initial optimization, and
747 AKS optimized further and carried out the experiments. AKS carried out the all analysis
748 and quantification of the data with respect to the effect of inhibitors on FtsZ assembly.
749 SMP carried out work related to 3D-SIM imaging, quantification, the resistance mutants
750 and the effect of inhibitors on yeast microtubules. JC carried out all the *in silico* work and
751 structural analysis. AKS, JC, GP and RS wrote the manuscript. AKS, SMP and JC edited
752 the draft manuscripts. SK contributed to the plotting and analysis of FRAP data. NM
753 carried out experiments related to MreB and A22 treatment.

754

755 **References**

756

757 Adams DW, Wu LJ, Czaplewski LG, Errington J. 2011. Multiple effects of benzamide
758 antibiotics on FtsZ function. *Mol Microbiol* **80**: 68–84.

759 Adams DW, Wu LJ, Errington J. 2016. A benzamide-dependent ftsZ mutant reveals
760 residues crucial for Z-ring assembly. *Mol Microbiol* **99**: 1028–1042.

761 Addinall SG, Holland B. 2002. The tubulin ancestor, FtsZ, draughtsman, designer and
762 driving force for bacterial cytokinesis. *J Mol Biol* **318**: 219–236.

763 Addinall SG, Lutkenhaus J. 1996. FtsZ-spirals and -arcs determine the shape of the
764 invaginating septa in some mutants of Escherichia coli. *Mol Microbiol* **22**: 231–237.

765 Agard D. 1984. Optical sectioning microscopy: cellular architecture in three dimensions.
766 *Annu Rev Biophys Biomol Struct* **13**: 191–219.

767 Anderson DE, Gueiros-Filho FJ, Erickson HP. 2004. Assembly dynamics of FtsZ rings in
768 Bacillus subtilis and Escherichia coli and effects of FtsZ-regulating proteins. *J Bacteriol*
769 **186**: 5775–5781.

770 Anderson DE, Kim MB, Moore JT, O'Brien TE, Sorto NA, Grove CI, Lackner LL, Ames JB,
771 Shaw JT. 2012. Comparison of small molecule inhibitors of the bacterial cell division
772 protein FtsZ and identification of a reliable cross-species inhibitor. *ACS Chem Biol* **7**:
773 1918–1928.

774 Andreu JM, Huecas S, Araújo-Bazán L, Vázquez-Villa H, Martín-Fontecha M. 2022. The
775 search for antibacterial inhibitors targeting cell division protein ftsz at its nucleotide and
776 allosteric binding sites. *Biomedicines* **10**.

777 Andreu JM, Schaffner-Barbero C, Huecas S, Alonso D, Lopez-Rodriguez ML, Ruiz-Avila
778 LB, Núñez-Ramírez R, Llorca O, Martín-Galiano AJ. 2010. The antibacterial cell division
779 inhibitor PC190723 is an FtsZ polymer-stabilizing agent that induces filament assembly
780 and condensation. *J Biol Chem* **285**: 14239–14246.

781 Araújo-Bazán L, Huecas S, Valle J, Andreu D, Andreu JM. 2019. Synthetic developmental
782 regulator MciZ targets FtsZ across Bacillus species and inhibits bacterial division. *Mol*
783 *Microbiol* **111**: 965–980.

784 Araújo-Bazán L, Ruiz-Avila LB, Andreu D, Huecas S, Andreu JM. 2016. Cytological profile
785 of antibacterial ftsz inhibitors and synthetic peptide mciz. *Front Microbiol* **7**: 1558.

786 Bähler J, Wu J-Q, Longtine MS, Shah NG, Mckenzie III A, Steever AB, Wach A, Philippsen
787 P, Pringle JR. 1998. Heterologous modules for efficient and versatile PCR-based gene
788 targeting in *Schizosaccharomyces pombe*. *Yeast* **14**: 943–951.

789 Balzi E, Goffeau A. 1991. Multiple or pleiotropic drug resistance in yeast. *Biochimica et*
790 *Biophysica Acta (BBA) - General Subjects* **1073**: 241–252.

791 Barrows JM, Goley ED. 2021. FtsZ dynamics in bacterial division: What, how, and why?
792 *Curr Opin Cell Biol* **68**: 163–172.

793 Basi G, Schmid E, Maundrell K. 1993. TATA box mutations in the Schizosaccharomyces
794 pombe nmt1 promoter affect transcription efficiency but not the transcription start point
795 or thiamine repressibility. *Gene* **123**: 131–136.

796 Benko Z, Liang D, Li G, Elder RT, Sarkar A, Takayama J, Ghosh AK, Zhao RY. 2017. A
797 fission yeast cell-based system for multidrug resistant HIV-1 proteases. *Cell Biosci* **7**: 5.

798 Benko Z, Zhang J, Zhao RY. 2019. Development of A Fission Yeast Cell-Based Platform
799 for High Throughput Screening of HIV-1 Protease Inhibitors. *Curr HIV Res* **17**: 429–440.

800 Beuria TK, Santra MK, Panda D. 2005. Sanguinarine blocks cytokinesis in bacteria by
801 inhibiting FtsZ assembly and bundling. *Biochemistry* **44**: 16584–16593.

802 Bi EF, Lutkenhaus J. 1991. FtsZ ring structure associated with division in Escherichia coli.
803 *Nature* **354**: 161–164.

804 Boberek JM, Stach J, Good L. 2010. Genetic evidence for inhibition of bacterial division
805 protein FtsZ by berberine. *PLoS ONE* **5**: e13745.

806 Bramhill D, Thompson CM. 1994. GTP-dependent polymerization of Escherichia coli FtsZ
807 protein to form tubules. *Proc Natl Acad Sci USA* **91**: 5813–5817.

808 Butler MS, Paterson DL. 2020. Antibiotics in the clinical pipeline in October 2019. *J*
809 *Antibiot* **73**: 329–364.

810 Carro L. 2019. Recent Progress in the Development of Small-Molecule FtsZ Inhibitors as
811 Chemical Tools for the Development of Novel Antibiotics. *Antibiotics (Basel)* **8**.

812 Casiraghi A, Suigo L, Valoti E, Straniero V. 2020. Targeting Bacterial Cell Division: A
813 Binding Site-Centered Approach to the Most Promising Inhibitors of the Essential
814 Protein FtsZ. *Antibiotics (Basel)* **9**.

815 Cernáková M, Kostálová D. 2002. Antimicrobial activity of berberine--a constituent of
816 Mahonia aquifolium. *Folia Microbiol (Praha)* **47**: 375–378.

817 Chai WC, Whittall JJ, Song D, Polyak SW, Ogunniyi AD, Wang Y, Bi F, Ma S, Semple SJ,
818 Venter H. 2020. Antimicrobial action and reversal of resistance in MRSA by
819 difluorobenzamide derivatives targeted at FtsZ. *Antibiotics (Basel)* **9**.

820 Chan F-Y, Sun N, Neves MAC, Lam PC-H, Chung W-H, Wong L-K, Chow H-Y, Ma D-L,
821 Chan P-H, Leung Y-C, et al. 2013. Identification of a new class of FtsZ inhibitors by
822 structure-based design and in vitro screening. *J Chem Inf Model* **53**: 2131–2140.

823 Chu M, Zhang M-B, Liu Y-C, Kang J-R, Chu Z-Y, Yin K-L, Ding L-Y, Ding R, Xiao R-X, Yin
824 Y-N, et al. 2016. Role of Berberine in the Treatment of Methicillin-Resistant
825 Staphylococcus aureus Infections. *Sci Rep* **6**: 24748.

826 Claridge-Chang A, Assam PN. 2016. Estimation statistics should replace significance
827 testing. *Nat Methods* **13**: 108–109.

828 Cumming G, Fidler F, Vaux DL. 2007. Error bars in experimental biology. *J Cell Biol* **177**:
829 7–11.

830 Di Somma A, Avitabile C, Cirillo A, Moretta A, Merlino A, Paduano L, Duilio A, Romanelli
831 A. 2020. The antimicrobial peptide Temporin L impairs E. coli cell division by interacting
832 with FtsZ and the divisome complex. *Biochim Biophys Acta Gen Subj* **1864**: 129606.

833 Domadia P, Swarup S, Bhunia A, Sivaraman J, Dasgupta D. 2007. Inhibition of bacterial
834 cell division protein FtsZ by cinnamaldehyde. *Biochem Pharmacol* **74**: 831–840.

835 Domadia PN, Bhunia A, Sivaraman J, Swarup S, Dasgupta D. 2008. Berberine targets
836 assembly of Escherichia coli cell division protein FtsZ. *Biochemistry* **47**: 3225–3234.

837 Elsen NL, Lu J, Parthasarathy G, Reid JC, Sharma S, Soisson SM, Lumb KJ. 2012.
838 Mechanism of action of the cell-division inhibitor PC190723: modulation of FtsZ
839 assembly cooperativity. *J Am Chem Soc* **134**: 12342–12345.

840 Erickson HP, Anderson DE, Osawa M. 2010. FtsZ in bacterial cytokinesis: cytoskeleton
841 and force generator all in one. *Microbiol Mol Biol Rev* **74**: 504–528.

842 Erickson HP. 1995. FtsZ, a prokaryotic homolog of tubulin? *Cell* **80**: 367–370.

843 Fujita J, Maeda Y, Mizohata E, Inoue T, Kaul M, Parhi AK, LaVoie EJ, Pilch DS,
844 Matsumura H. 2017. Structural Flexibility of an Inhibitor Overcomes Drug Resistance
845 Mutations in Staphylococcus aureus FtsZ. *ACS Chem Biol* **12**: 1947–1955.

846 Gitai Z, Dye NA, Reisenauer A, Wachi M, Shapiro L. 2005. MreB actin-mediated
847 segregation of a specific region of a bacterial chromosome. *Cell* **120**: 329–341.

848 Haydon DJ, Stokes NR, Ure R, Galbraith G, Bennett JM, Brown DR, Baker PJ, Barynin
849 VV, Rice DW, Sedelnikova SE, et al. 2008. An inhibitor of FtsZ with potent and selective
850 anti-staphylococcal activity. *Science* **321**: 1673–1675.

851 Henty-Ridilla JL, Li J, Day B, Staiger CJ. 2014. ACTIN DEPOLYMERIZING FACTOR4
852 regulates actin dynamics during innate immune signaling in Arabidopsis. *Plant Cell* **26**:
853 340–352.

854 Hernández-Rocamora VM, Alfonso C, Margolin W, Zorrilla S, Rivas G. 2015. Evidence
855 that bacteriophage λ kil peptide inhibits bacterial cell division by disrupting ftsz
856 protofilaments and sequestering protein subunits. *J Biol Chem* **290**: 20325–20335.

857 Higaki T. 2017. Quantitative evaluation of cytoskeletal organizations by microscopic image
858 analysis. *PLANT MORPHOL* **29**: 15–21.

859 Hou S, Wieczorek SA, Kaminski TS, Ziebacz N, Tabaka M, Sorto NA, Foss MH, Shaw JT,
860 Thanbichler M, Weibel DB, et al. 2012. Characterization of Caulobacter crescentus FtsZ
861 protein using dynamic light scattering. *J Biol Chem* **287**: 23878–23886.

862 Ho J, Tumkaya T, Aryal S, Choi H, Claridge-Chang A. 2019. Moving beyond P values:
863 data analysis with estimation graphics. *Nat Methods* **16**: 565–566.

864 Huang K-H, Durand-Heredia J, Janakiraman A. 2013. FtsZ ring stability: of bundles,
865 tubules, crosslinks, and curves. *J Bacteriol* **195**: 1859–1868.

866 Huecas S, Ramírez-Aportela E, Vergoñós A, Núñez-Ramírez R, Llorca O, Díaz JF, Juan-
867 Rodríguez D, Oliva MA, Castellen P, Andreu JM. 2017. Self-Organization of FtsZ
868 Polymers in Solution Reveals Spacer Role of the Disordered C-Terminal Tail. *Biophys J*
869 **113**: 1831–1844.

870 Hurley KA, Santos TM, Nepomuceno GM, Huynh V, Shaw JT, Weibel DB. 2016. Targeting
871 the bacterial division protein FtsZ. *J Med Chem* **59**: 6975–6998.

872 Irwin JJ, Duan D, Torosyan H, Doak AK, Ziebart KT, Sterling T, Tumanian G, Shoichet BK.
873 2015. An aggregation advisor for ligand discovery. *J Med Chem* **58**: 7076–7087.

874 Iwai N, Nagai K, Wachi M. 2002. Novel S-benzylisothiourea compound that induces
875 spherical cells in Escherichia coli probably by acting on a rod-shape-determining
876 protein(s) other than penicillin-binding protein 2. *Biosci Biotechnol Biochem* **66**: 2658–
877 2662.

878 Kaul M, Mark L, Zhang Y, Parhi AK, LaVoie EJ, Pilch DS. 2013a. Pharmacokinetics and in
879 vivo antistaphylococcal efficacy of TXY541, a 1-methylpiperidine-4-carboxamide prodrug
880 of PC190723. *Biochem Pharmacol* **86**: 1699–1707.

881 Kaul M, Parhi AK, Zhang Y, LaVoie EJ, Tuske S, Arnold E, Kerrigan JE, Pilch DS. 2012. A
882 bactericidal guanidinomethyl biaryl that alters the dynamics of bacterial FtsZ
883 polymerization. *J Med Chem* **55**: 10160–10176.

884 Kaul M, Zhang Y, Parhi AK, Lavoie EJ, Pilch DS. 2014. Inhibition of RND-type efflux
885 pumps confers the FtsZ-directed prodrug TXY436 with activity against Gram-negative
886 bacteria. *Biochem Pharmacol* **89**: 321–328.

887 Kaul M, Zhang Y, Parhi AK, Lavoie EJ, Tuske S, Arnold E, Kerrigan JE, Pilch DS. 2013b.
888 Enterococcal and streptococcal resistance to PC190723 and related compounds:
889 molecular insights from a FtsZ mutational analysis. *Biochimie* **95**: 1880–1887.

890 Kelley C, Zhang Y, Parhi A, Kaul M, Pilch DS, LaVoie EJ. 2012. 3-Phenyl substituted 6,7-
891 dimethoxyisoquinoline derivatives as FtsZ-targeting antibacterial agents. *Bioorg Med*
892 *Chem* **20**: 7012–7029.

893 Khare S, Hsin J, Sorto NA, Nepomuceno GM, Shaw JT, Shi H, Huang KC. 2019. FtsZ-
894 Independent Mechanism of Division Inhibition by the Small Molecule PC190723 in
895 Escherichia coli. *Adv Biosys* **3**: e1900021.

896 Kumar K, Awasthi D, Lee S-Y, Zanardi I, Ruzsicska B, Knudson S, Tonge PJ, Slayden RA,
897 Ojima I. 2011. Novel trisubstituted benzimidazoles, targeting Mtb FtsZ, as a new class of
898 antitubercular agents. *J Med Chem* **54**: 374–381.

899 Kusuma KD, Payne M, Ung AT, Bottomley AL, Harry EJ. 2019. FtsZ as an antibacterial
900 target: status and guidelines for progressing this avenue. *ACS Infect Dis* **5**: 1279–1294.

901 Läppchen T, Pinas VA, Hartog AF, Koomen G-J, Schaffner-Barbero C, Andreu JM,
902 Trambaiolo D, Löwe J, Juhem A, Popov AV, et al. 2008. Probing FtsZ and tubulin with
903 C8-substituted GTP analogs reveals differences in their nucleotide binding sites. *Chem*
904 *Biol* **15**: 189–199.

905 Liu F, Venter H, Bi F, Semple SJ, Liu J, Jin C, Ma S. 2017. Synthesis and antibacterial
906 activity of 5-methylphenanthridium derivatives as FtsZ inhibitors. *Bioorg Med Chem Lett*
907 **27**: 3399–3402.

908 Li X, Sheng J, Huang G, Ma R, Yin F, Song D, Zhao C, Ma S. 2015. Design, synthesis and
909 antibacterial activity of cinnamaldehyde derivatives as inhibitors of the bacterial cell
910 division protein FtsZ. *Eur J Med Chem* **97**: 32–41.

911 Lopus M, Panda D. 2006. The benzophenanthridine alkaloid sanguinarine perturbs
912 microtubule assembly dynamics through tubulin binding. A possible mechanism for its
913 antiproliferative activity. *FEBS J* **273**: 2139–2150.

914 Lord SJ, Velle KB, Mullins RD, Fritz-Laylin LK. 2020. SuperPlots: Communicating
915 reproducibility and variability in cell biology. *J Cell Biol* **219**.

916 Löwe J, Amos LA. 1998. Crystal structure of the bacterial cell-division protein FtsZ. *Nature*
917 **391**: 203–206.

918 Lui HK, Gao W, Cheung KC, Jin WB, Sun N, Kan JWY, Wong ILK, Chiou J, Lin D, Chan
919 EWC, et al. 2019. Boosting the efficacy of anti-MRSA β-lactam antibiotics via an easily

920 accessible, non-cytotoxic and orally bioavailable FtsZ inhibitor. *Eur J Med Chem* **163**:
921 95–115.

922 Mahone CR, Goley ED. 2020. Bacterial cell division at a glance. *J Cell Sci* **133**.

923 Margalit DN, Romberg L, Mets RB, Hebert AM, Mitchison TJ, Kirschner MW,
924 RayChaudhuri D. 2004. Targeting cell division: small-molecule inhibitors of FtsZ
925 GTPase perturb cytokinetic ring assembly and induce bacterial lethality. *Proc Natl Acad*
926 *Sci USA* **101**: 11821–11826.

927 Margolin W. 2005. FtsZ and the division of prokaryotic cells and organelles. *Nat Rev Mol*
928 *Cell Biol* **6**: 862–871.

929 Martin JK, Sheehan JP, Bratton BP, Moore GM, Mateus A, Li SH-J, Kim H, Rabinowitz JD,
930 Typas A, Savitski MM, et al. 2020. A Dual-Mechanism Antibiotic Kills Gram-Negative
931 Bacteria and Avoids Drug Resistance. *Cell* **181**: 1518-1532.e14.

932 Matsui T, Yamane J, Mogi N, Yamaguchi H, Takemoto H, Yao M, Tanaka I. 2012a.
933 Structural reorganization of the bacterial cell-division protein FtsZ from Staphylococcus
934 aureus. *Acta Crystallogr D Biol Crystallogr* **68**: 1175–1188.

935 Matsui T, Yamane J, Mogi N, Yamaguchi H, Takemoto H, Yao M, Tanaka I. 2012b.
936 Structural reorganization of the bacterial cell-division protein FtsZ from Staphylococcus
937 aureus. *Acta Crystallogr D Biol Crystallogr* **68**: 1175–1188.

938 Ma X, Ehrhardt DW, Margolin W. 1996. Colocalization of cell division proteins FtsZ and
939 FtsA to cytoskeletal structures in living Escherichia coli cells by using green fluorescent
940 protein. *Proc Natl Acad Sci USA* **93**: 12998–13003.

941 Miguel A, Hsin J, Liu T, Tang G, Altman RB, Huang KC. 2015. Variations in the binding
942 pocket of an inhibitor of the bacterial division protein FtsZ across genotypes and
943 species. *PLoS Comput Biol* **11**: e1004117.

944 Mikuni S, Kodama K, Sasaki A, Kohira N, Maki H, Munetomo M, Maenaka K, Kinjo M.
945 2015. Screening for FtsZ Dimerization Inhibitors Using Fluorescence Cross-Correlation
946 Spectroscopy and Surface Resonance Plasmon Analysis. *PLoS ONE* **10**: e0130933.

947 Monahan LG, Robinson A, Harry EJ. 2009. Lateral FtsZ association and the assembly of
948 the cytokinetic Z ring in bacteria. *Mol Microbiol* **74**: 1004–1017.

949 Monterroso B, Alfonso C, Zorrilla S, Rivas G. 2013. Combined analytical
950 ultracentrifugation, light scattering and fluorescence spectroscopy studies on the
951 functional associations of the bacterial division FtsZ protein. *Methods* **59**: 349–362.

952 Moreno MB, Durán A, Carlos Ribas J. 2000. A family of multifunctional thiamine-
953 repressible expression vectors for fission yeast. *Yeast* **16**: 861–872.

954 Mukherjee A, Cao C, Lutkenhaus J. 1998. Inhibition of FtsZ polymerization by SulA, an
955 inhibitor of septation in Escherichia coli. *Proc Natl Acad Sci USA* **95**: 2885–2890.

956 Mukherjee A, Lutkenhaus J. 1999. Analysis of FtsZ assembly by light scattering and
957 determination of the role of divalent metal cations. *J Bacteriol* **181**: 823–832.

958 Nepomuceno GM, Chan KM, Huynh V, Martin KS, Moore JT, O'Brien TE, Pollo LAE,
959 Sarabia FJ, Tadeus C, Yao Z, et al. 2015. Synthesis and evaluation of quinazolines as
960 inhibitors of the bacterial cell division protein ftsz. *ACS Med Chem Lett* **6**: 308–312.

961 Nogales E, Downing KH, Amos LA, Löwe J. 1998. Tubulin and FtsZ form a distinct family
962 of GTPases. *Nat Struct Biol* **5**: 451–458.

963 Nonejuie P, Burkart M, Pogliano K, Pogliano J. 2013. Bacterial cytological profiling rapidly
964 identifies the cellular pathways targeted by antibacterial molecules. *Proc Natl Acad Sci*
965 *USA* **110**: 16169–16174.

966 Nova E, Montecinos F, Brunet JE, Lagos R, Monasterio O. 2007. 4',6-Diamidino-2-
967 phenylindole (DAPI) induces bundling of Escherichia coli FtsZ polymers inhibiting the
968 GTPase activity. *Arch Biochem Biophys* **465**: 315–319.

969 Obiang-Obounou BW, Kang O-H, Choi J-G, Keum J-H, Kim S-B, Mun S-H, Shin D-W, Kim
970 KW, Park C-B, Kim Y-G, et al. 2011. The mechanism of action of sanguinarine against
971 methicillin-resistant Staphylococcus aureus. *J Toxicol Sci* **36**: 277–283.

972 Pande V, Mitra N, Bagde SR, Srinivasan R, Gayathri P. 2022. Filament organization of the
973 bacterial actin MreB is dependent on the nucleotide state. *J Cell Biol* **221**.

974 Park B, Awasthi D, Chowdhury SR, Melief EH, Kumar K, Knudson SE, Slayden RA, Ojima
975 I. 2014. Design, synthesis and evaluation of novel 2,5,6-trisubstituted benzimidazoles
976 targeting FtsZ as antitubercular agents. *Bioorg Med Chem* **22**: 2602–2612.

977 Pérez P, Ribas JC. 2004. Cell wall analysis. *Methods* **33**: 245–251.

978 Pettersen EF, Goddard TD, Huang CC, Couch GS, Greenblatt DM, Meng EC, Ferrin TE.
979 2004. UCSF Chimera—a visualization system for exploratory research and analysis. *J*
980 *Comput Chem* **25**: 1605–1612.

981 Piddock LJV. 2006. Clinically relevant chromosomally encoded multidrug resistance efflux
982 pumps in bacteria. *Clin Microbiol Rev* **19**: 382–402.

983 Pierpaoli E, Cirioni O, Simonetti O, Orlando F, Giacometti A, Lombardi P, Provinciali M.
984 2021. Potential application of berberine in the treatment of Escherichia coli sepsis. *Nat*
985 *Prod Res* **35**: 4779–4784.

986 Pollard DA, Pollard TD, Pollard KS. 2019. Empowering statistical methods for cellular and
987 molecular biologists. *Mol Biol Cell* **30**: 1359–1368.

988 Popp D, Iwasa M, Narita A, Erickson HP, Maéda Y. 2009. FtsZ condensates: an in vitro
989 electron microscopy study. *Biopolymers* **91**: 340–350.

990 Pradhan P, Margolin W, Beuria TK. 2021. Targeting the achilles heel of ftsz: the
991 interdomain cleft. *Front Microbiol* **12**: 732796.

992 Raghav D, Ashraf SM, Mohan L, Rathinasamy K. 2017. Berberine Induces Toxicity in
993 HeLa Cells through Perturbation of Microtubule Polymerization by Binding to Tubulin at
994 a Unique Site. *Biochemistry* **56**: 2594–2611.

995 Rai D, Singh JK, Roy N, Panda D. 2008. Curcumin inhibits FtsZ assembly: an attractive
996 mechanism for its antibacterial activity. *Biochem J* **410**: 147–155.

997 RayChaudhuri D, Park JT. 1992. Escherichia coli cell-division gene ftsZ encodes a novel
998 GTP-binding protein. *Nature* **359**: 251–254.

999 Reija B, Monterroso B, Jiménez M, Vicente M, Rivas G, Zorrilla S. 2011. Development of a
1000 homogeneous fluorescence anisotropy assay to monitor and measure FtsZ assembly in
1001 solution. *Anal Biochem* **418**: 89–96.

1002 Rivas G, Vogel SK, Schwille P. 2014. Reconstitution of cytoskeletal protein assemblies for
1003 large-scale membrane transformation. *Curr Opin Chem Biol* **22**: 18–26.

1004 Rosado-Lugo JD, Sun Y, Banerjee A, Cao Y, Datta P, Zhang Y, Yuan Y, Parhi AK. 2022.
1005 Evaluation of 2,6-difluoro-3-(oxazol-2-ylmethoxy)benzamide chemotypes as Gram-
1006 negative FtsZ inhibitors. *J Antibiot* **75**: 385–395.

1007 Ruiz-Avila LB, Huecas S, Artola M, Vergoñós A, Ramírez-Aportela E, Cercenado E,
1008 Barasoain I, Vázquez-Villa H, Martín-Fontecha M, Chacón P, et al. 2013. Synthetic
1009 inhibitors of bacterial cell division targeting the GTP-binding site of FtsZ. *ACS Chem Biol*
1010 **8**: 2072–2083.

1011 Schaffner-Barbero C, Martín-Fontecha M, Chacón P, Andreu JM. 2012. Targeting the
1012 assembly of bacterial cell division protein FtsZ with small molecules. *ACS Chem Biol* **7**:
1013 269–277.

1014 Schindelin J, Arganda-Carreras I, Frise E, Kaynig V, Longair M, Pietzsch T, Preibisch S,
1015 Rueden C, Saalfeld S, Schmid B, et al. 2012. Fiji: an open-source platform for biological-
1016 image analysis. *Nat Methods* **9**: 676–682.

1017 Sievers F, Wilm A, Dineen D, Gibson TJ, Karplus K, Li W, Lopez R, McWilliam H,
1018 Remmert M, Söding J, et al. 2011. Fast, scalable generation of high-quality protein
1019 multiple sequence alignments using Clustal Omega. *Mol Syst Biol* **7**: 539.

1020 Silber N, Matos de Opitz CL, Mayer C, Sass P. 2020. Cell division protein FtsZ: from
1021 structure and mechanism to antibiotic target. *Future Microbiol* **15**: 801–831.

1022 Spahn C, Gómez-de-Mariscal E, Laine RF, Pereira PM, von Chamier L, Conduit M, Pinho
1023 MG, Jacquemet G, Holden S, Heilemann M, et al. 2022. DeepBacs for multi-task
1024 bacterial image analysis using open-source deep learning approaches. *Commun Biol* **5**:
1025 688.

1026 Specht M, Dempwolff F, Schätzle S, Thomann R, Waidner B. 2013. Localization of FtsZ in
1027 Helicobacter pylori and consequences for cell division. *J Bacteriol* **195**: 1411–1420.

1028 Srinivasan R, Mishra M, Murata-Hori M, Balasubramanian MK. 2007. Filament formation of
1029 the Escherichia coli actin-related protein, MreB, in fission yeast. *Curr Biol* **17**: 266–272.

1030 Srinivasan R, Mishra M, Wu L, Yin Z, Balasubramanian MK. 2008. The bacterial cell
1031 division protein FtsZ assembles into cytoplasmic rings in fission yeast. *Genes Dev* **22**:
1032 1741–1746.

1033 Stokes NR, Baker N, Bennett JM, Berry J, Collins I, Czaplewski LG, Logan A, Macdonald
1034 R, Macleod L, Peasley H, et al. 2013. An improved small-molecule inhibitor of FtsZ with
1035 superior in vitro potency, drug-like properties, and in vivo efficacy. *Antimicrob Agents*
1036 *Chemother* **57**: 317–325.

1037 Strahl H, Hamoen LW. 2010. Membrane potential is important for bacterial cell division.
1038 *Proc Natl Acad Sci USA* **107**: 12281–12286.

1039 Straniero V, Sebastián-Pérez V, Hrast M, Zanotto C, Casiraghi A, Suigo L, Zdovc I,
1040 Radaelli A, De Giuli Morghen C, Valoti E. 2020a. Benzodioxane-Benzamides as
1041 Antibacterial Agents: Computational and SAR Studies to Evaluate the Influence of the 7-
1042 Substitution in FtsZ Interaction. *ChemMedChem* **15**: 195–209.

1043 Straniero V, Suigo L, Casiraghi A, Sebastián-Pérez V, Hrast M, Zanotto C, Zdovc I, De
1044 Giuli Morghen C, Radaelli A, Valoti E. 2020b. Benzamide derivatives targeting the cell
1045 division protein ftsz: modifications of the linker and the benzodioxane scaffold and their
1046 effects on antimicrobial activity. *Antibiotics (Basel)* **9**.

1047 Straniero V, Zanotto C, Straniero L, Casiraghi A, Duga S, Radaelli A, De Giuli Morghen C,
1048 Valoti E. 2017. 2,6-Difluorobenzamide Inhibitors of Bacterial Cell Division Protein FtsZ:
1049 Design, Synthesis, and Structure-Activity Relationships. *ChemMedChem* **12**: 1303–
1050 1318.

1051 Sun N, Chan F-Y, Lu Y-J, Neves MAC, Lui H-K, Wang Y, Chow K-Y, Chan K-F, Yan S-C,
1052 Leung Y-C, et al. 2014. Rational design of berberine-based FtsZ inhibitors with broad-
1053 spectrum antibacterial activity. *PLoS ONE* **9**: e97514.

1054 Sun N, Lu Y-J, Chan F-Y, Du R-L, Zheng Y-Y, Zhang K, So L-Y, Abagyan R, Zhuo C,
1055 Leung Y-C, et al. 2017. A thiazole orange derivative targeting the bacterial protein ftsz
1056 shows potent antibacterial activity. *Front Microbiol* **8**: 855.

1057 Tan CM, Therien AG, Lu J, Lee SH, Caron A, Gill CJ, Lebeau-Jacob C, Benton-Perdomo
1058 L, Monteiro JM, Pereira PM, et al. 2012. Restoring methicillin-resistant Staphylococcus
1059 aureus susceptibility to β-lactam antibiotics. *Sci Transl Med* **4**: 126ra35.

1060 TAXIS Pharmaceuticals. 2020. TAXIS secures NIH Funding – TAXIS Pharmaceutical.
1061 https://www.taxispharma.com/news/taxis-secures-nih-funding/ (Accessed February 8,
1062 2022).

1063 TerBush AD, MacCready JS, Chen C, Ducat DC, Osteryoung KW. 2018. Conserved
1064 dynamics of chloroplast cytoskeletal ftsz proteins across photosynthetic lineages. *Plant*
1065 *Physiol* **176**: 295–306.

1066 TerBush AD, Osteryoung KW. 2012. Distinct functions of chloroplast FtsZ1 and FtsZ2 in Z-
1067 ring structure and remodeling. *J Cell Biol* **199**: 623–637.

1068 Tripathy S, Sahu SK. 2019. FtsZ inhibitors as a new genera of antibacterial agents. *Bioorg*
1069 *Chem* **91**: 103169.

1070 van den Ent F, Löwe J. 2006. RF cloning: a restriction-free method for inserting target
1071 genes into plasmids. *J Biochem Biophys Methods* **67**: 67–74.

1072 Vaughan S, Wickstead B, Gull K, Addinall SG. 2004. Molecular evolution of FtsZ protein
1073 sequences encoded within the genomes of archaea, bacteria, and eukaryota. *J Mol Evol*
1074 **58**: 19–29.

1075 Vaux DL. 2014. Basic statistics in cell biology. *Annu Rev Cell Dev Biol* **30**: 23–37.

1076 Vollmer W. 2006. The prokaryotic cytoskeleton: a putative target for inhibitors and
1077 antibiotics? *Appl Microbiol Biotechnol* **73**: 37–47.

1078 von Chamier L, Laine RF, Jukkala J, Spahn C, Krentzel D, Nehme E, Lerche M,
1079 Hernández-Pérez S, Mattila PK, Karinou E, et al. 2021. Democratising deep learning for
1080 microscopy with ZeroCostDL4Mic. *Nat Commun* **12**: 2276.

1081 Wang J, Galgoci A, Kodali S, Herath KB, Jayasuriya H, Dorso K, Vicente F, González A,
1082 Cully D, Bramhill D, et al. 2003. Discovery of a small molecule that inhibits cell division
1083 by blocking FtsZ, a novel therapeutic target of antibiotics. *J Biol Chem* **278**: 44424–
1084 44428.

1085 Wang J, Ma W, Fang Y, Liang H, Yang H, Wang Y, Dong X, Zhan Y, Wang X. 2021. Core
1086 Oligosaccharide Portion of Lipopolysaccharide Plays Important Roles in Multiple
1087 Antibiotic Resistance in Escherichia coli. *Antimicrob Agents Chemother* **65**: e0034121.

1088 Wang X, Tanaka M, Krstin S, Peixoto HS, Wink M. 2016. The Interference of Selected
1089 Cytotoxic Alkaloids with the Cytoskeleton: An Insight into Their Modes of Action.
1090 *Molecules* **21**.

1091 Wang Y, Yan M, Ma R, Ma S. 2015. Synthesis and antibacterial activity of novel 4-bromo-
1092 1H-indazole derivatives as FtsZ inhibitors. *Arch Pharm (Weinheim)* **348**: 266–274.

1093 Waterhouse A, Bertoni M, Bienert S, Studer G, Tauriello G, Gumienny R, Heer FT, de
1094 Beer TAP, Rempfer C, Bordoli L, et al. 2018. SWISS-MODEL: homology modelling of
1095 protein structures and complexes. *Nucleic Acids Res* **46**: W296–W303.

1096 Waterhouse AM, Procter JB, Martin DMA, Clamp M, Barton GJ. 2009. Jalview Version 2--
1097 a multiple sequence alignment editor and analysis workbench. *Bioinformatics* **25**: 1189–
1098 1191.

1099 Weiss DS, Chen JC, Ghigo JM, Boyd D, Beckwith J. 1999. Localization of FtsI (PBP3) to
1100 the septal ring requires its membrane anchor, the Z ring, FtsA, FtsQ, and FtsL. *J*
1101 *Bacteriol* **181**: 508–520.

1102 Weiss DS. 2004. Bacterial cell division and the septal ring. *Mol Microbiol* **54**: 588–597.

1103 Wolff J, Knipling L. 1993. Antimicrotubule properties of benzophenanthridine alkaloids.
1104 *Biochemistry* **32**: 13334–13339.

1105 Yoshida Y, Mogi Y, TerBush AD, Osteryoung KW. 2016. Chloroplast FtsZ assembles into
1106 a contractible ring via tubulin-like heteropolymerization. *Nat Plants* **2**: 16095.

1107 Zorrilla S, Monterroso B, Robles-Ramos M-Á, Margolin W, Rivas G. 2021. FtsZ
1108 interactions and biomolecular condensates as potential targets for new antibiotics.
1109 *Antibiotics (Basel)* **10**.

1110 **Figure Legends:**

1111

1112 **Figure 1. Polymerization of SaFtsZ, EcFtsZ and HpFtsZ in fission yeast.** The
1113 medium-strength *nmt42* promoter was used for the expression of different bacterial FtsZ-
1114 GFP fusion constructs in *S. pombe*. *S. pombe* cultures expressing FtsZ-GFP fusions were
1115 grown for 16–20 h at 30°C in the absence of thiamine to allow the expression of the
1116 proteins, mounted onto 1.6% agarose slide, and imaged using an **(A, B, E and D)**
1117 epifluorescence microscope or **(C and F)** super-resolution using 3D-SIM. **(A)** SaFtsZ and
1118 **(B)** EcFtsZ assembles into spots and cable-like structures in fission yeast (panels ii and
1119 iii). Arrows indicate ring-like structures. **(C)** 3D-SIM images of SaFtsZ. **(C i)** Maximum
1120 intensity projection image and **(C ii)** a single plane image reveal ring-like structures of
1121 SaFtsZ. Arrows indicate visible SaFtsZ rings. **(D)** HpFtsZ forms cable-like structures.
1122 Spiral filaments of HpFtsZ are indicated by white arrowheads, and linear cables are
1123 marked with yellow arrowheads. DIC or phase-contrast images are shown in **Ai, Bi & Di**.
1124 **(C)** Deconvolved image of HpFtsZ and **(F)** 3D-SIM images of HpFtsZ show the assembly
1125 of HpFtsZ into helical filaments in fission yeast. Scale bar represents 5 μm for all images
1126 **(A, B, D and F)** except for the image in **C** and **E**, where it represents 2.5 μm.

1127

1128

1129 **Figure 2. Inhibition of FtsZ polymerisation by sanguinarine and berberine.** Fission
1130 yeast cultures expressing different bacterial FtsZ-GFP fusions were grown at 30ºC in the
1131 absence of thiamine for 10 – 12 hours before DMSO or drugs were added to the cultures.
1132 The cultures were further grown at 30ºC for another 10 – 12 hours, either in the absence
1133 or presence of the drug before imaging or counting. Cells were mounted onto 1.6%
1134 agarose slides, and an epifluorescence microscope was used for the imaging. In control
1135 (untreated) cultures, an equivalent amount of DMSO was added. **(A i – C i)** Control
1136 (DMSO-treated) cells showed normal assembly of FtsZ polymers in fission yeast. **(A i)**
1137 SaFtsZ **(B i)** EcFtsZ and **(C i)** HpFtsZ. **(A ii – C ii)** Sanguinarine (20 μM) treated cells
1138 showed a significant reduction in **(A ii)** SaFtsZ, **(B ii)** EcFtsZ and **(C ii)** HpFtsZ. **(A iii – C**
1139 **iii)** Berberine (53.79 μM) inhibited the polymerization of **(A iii)** SaFtsZ, **(B iii)** EcFtsZ and
1140 **(C iii)** HpFtsZ. Scale bar represents 5 μm. **(D – G)** Quantification of the effects of
1141 sanguinarine **(D and E)** and berberine **(F and G)** on polymerization of SaFtsZ **(i)**, EcFtsZ
1142 **(ii)** and HpFtsZ **(iii)**, respectively. **(D and F)** show the percentage of cells having polymers
1143 in the presence or absence of sanguinarine **(D)** or berberine **(F)**. Light gray bars and dark
1144 gray bars represent cells having diffuse fluorescence and cells containing FtsZ polymers,
1145 respectively. **(E and G)** Superplots showing the quantification of the number of spots per
1146 cell and density, which is a measure for the amount of assembled cytoskeleton per unit
1147 area in a given cell for **(i)** SaFtsZ or **(ii)** EcFtsZ or total polymer length per cell for and
1148 density for **(iii)** HpFtsZ when treated with **(E)** sanguinarine or **(G)** berberine. For the
1149 quantification of spots in **(E)**, the number of cells counted for each replicate for SaFtsZ and
1150 EcFtsZ were ≥ 44 and ≤ 72; N = 3 and ≥ 64 and ≤ 130; N = 3, respectively. In the case of
1151 HpFtsZ, polymer length per cell was measured from ≥ 112 and ≤ 147 cells for each
1152 replicate (N = 4). For density measurement, the number of cells counted for each replicate
1153 for SaFtsZ, EcFtsZ, and HpFtsZ was ≥ 68 and ≤ 167; N = 3, ≥ 64 and ≤ 130; N = 3 and ≥
1154 112 and ≤ 147; N = 4 respectively. For the quantification of spots in **(G)**, the number of

1155 cells counted for each replicate for SaFtsZ and EcFtsZ were ≥ 42 and ≤ 82; N = 4 and ≥ 48
1156 and ≤ 136; N = 4, respectively. In the case of HpFtsZ, polymer length per cell was
1157 measured from ≥ 91 and ≤ 182 cells for each replicate (N = 3). For density measurement,
1158 the number of cells counted for each replicate for SaFtsZ, EcFtsZ, and HpFtsZ was ≥ 75
1159 and ≤ 151; N = 4, ≥ 48 and ≤ 136; N = 4 and ≥ 91 and ≤ 182; N = 3 respectively. The
1160 black bars represent the mean values derived from independent biological replicates, the
1161 large markers represent the mean values of each replicate, and the small markers
1162 represent individual cells. The error bars shown are inferential and represent Mean ± 95%
1163 CI. Asterix ***, ** and * indicate P-values ≤ 0.001, ≤ 0.01 and < 0.05 respectively. P-
1164 values were calculated using the two-sided proportions z-test **(D and F)** or a two-sided
1165 unpaired Student's t-test **(E and G)**. The difference in the means between the untreated
1166 and treated populations is also indicated as effect size [95% CI, lower bound, upper
1167 bound]. Biological replicates are independent liquid cultures starting from a fresh patch of
1168 yeast cells grown from frozen glycerol stocks. **(H)** Berberine and sanguinarine, but not
1169 PC190723, affect yeast cell morphology at high concentrations. *S. pombe* cultures were
1170 grown **(i)** in the absence of the drug or in the presence of **(ii)** sanguinarine (135.95 μM) or
1171 **(iii)** berberine (134.45 μM) or **(iv)** PC190723 (140.6 μM) and mounted onto 1.6% agarose
1172 slides and imaged. In control (untreated) cultures, an equivalent amount of DMSO was
1173 added. Fission yeast cells formed bulges at the poles, as indicated by arrowheads. Scale
1174 bar represents 5 μm.
1175

1176 **Figure 3. PC190723 induces polymerization of SaFtsZ and HpFtsZ in fission yeast.**
1177 *S. pombe* cells expressing SaFtsZ, HpFtsZ or EcFtsZ were grown at 30ºC in the absence
1178 of thiamine for 8 – 10 hours before DMSO or PC190723 was added to the cultures. The
1179 cultures were further incubated at 30ºC for 4 hours before imaging or counting. **(A)** Dose-
1180 dependent effect of PC190723 on polymerization of SaFtsZ. Graph showing percentage
1181 of cells having diffuse (light gray) and polymerized (dark gray) SaFtsZ in fission yeast in
1182 the absence (DMSO) or in the presence of PC190723 ranging from 14.06 – 70.27 μM
1183 concentration. **(B)** Images showing the effect of PC190723 at 56.2 μM on SaFtsZ. At a
1184 time-point when control (DMSO treated) cells expressing SaFtsZ-GFP show diffuse
1185 fluorescence (panel ii), cells grown with PC190723 (56.2 μM) result in the early
1186 appearance of SaFtsZ assemblies (panel iv). **(C)** 3D-SIM images of SaFtsZ showing ring-
1187 like structures in both the absence **(i)** and presence **(ii)** of PC190723. **(D)** Dose-
1188 dependent effect of PC190723 on polymerization of HpFtsZ. Graph showing the
1189 percentage of cells having diffuse (light gray) and polymerized (dark gray) HpFtsZ in
1190 fission yeast in a range of PC190723 (14.06 – 70.27 μM) concentrations. **(E)** Images
1191 showing the effect of PC190723 at 56.2 μM on HpFtsZ. At a time-point when control
1192 (DMSO treated) cells expressing HpFtsZ-GFP show diffuse fluorescence (panel ii), cells
1193 grown with PC190723 (56.2 μM) result in the early appearance of HpFtsZ polymers (panel
1194 iv). **(F)** 3D-SIM images of HpFtsZ polymers showing spiral structures in both the absence
1195 **(i)** or presence **(ii)** of PC190723. **(G)** Superplots showing the quantification of the number
1196 of spots per cell and density (SaFtsZ), which is a measure for the amount of assembled
1197 cytoskeleton in a given cell in the presence or absence of PC190723. For the
1198 quantification of spots, the number of cells counted for each replicate was ≥ 18 and ≤ 85;
1199 N = 4, and for density measurement, the number of cells counted for each replicate was ≥
1200 86 and ≤ 176; N = 4. **(H)** Superplots for HpFtsZ showing the quantification and the effect
1201 of PC190723 on total polymer length per cell and density, a measure for the amount of

1202 assembled cytoskeleton per unit area in a given cell. For the quantification of polymer
1203 length and density measurement, the number of cells counted for each replicate was ≥ 104
1204 and ≤ 159; N = 4. **(I) and (J)** Images showing the effect of PC190723 at 56.2 μM on
1205 EcFtsZ. **(I)** Unlike Sa or HpFtsZ, cells expressing EcFtsZ-GFP and grown in the presence
1206 of PC190723 (56.2 μM) exhibit diffuse fluorescence similar to that of control (DMSO
1207 treated) cells at early time points. *S. pombe* cells expressing EcFtsZ were grown at 30ºC
1208 in the absence of thiamine for 4 – 6 hours before DMSO or PC190723 was added to the
1209 cultures. The cultures were further incubated for 4 hours at 30ºC before imaging or
1210 counting. **(J)** At longer induction times (20 hours), both control (DMSO) and PC190723
1211 treated cells formed EcFtsZ structures. DMSO or PC190723 was added to the cultures
1212 after 6 - 8 hours of growth in the absence of thiamine and incubated further at 30ºC. The
1213 black bars represent the mean values derived from independent biological replicates, the
1214 large markers represent the mean values of each replicate, and the small markers
1215 represent individual cells. The error bars shown in **A** and **D** are inferential and represent
1216 the 95% CI. ****, ***, ** and * indicate P-values ≤ 0.0001, ≤ 0.001, ≤ 0.01 and < 0.05
1217 respectively. P-values were calculated using the two-sided proportions z-test in **A** and **D**.
1218 A two-sided unpaired Student's t-test was used to calculate P-values in **G** and **H**. The
1219 difference in the means between the untreated and treated populations is also indicated as
1220 effect size [95% CI, lower bound, upper bound]. Scale bar represents 5 μm.
1221
1222

1223 **Figure 4. PC190723 reduces the polymer turnover rates of SaFtsZ and HpFtsZ.**
1224 Fluorescence recovery after photobleaching (FRAP) of **(A)** control (DMSO treated) and **(B)**
1225 PC190723 (56.2 μM) treated cells expressing SaFtsZ. Fission yeast cultures expressing
1226 SaFtsZ-GFP were mounted onto agarose slides and imaged with an epifluorescence
1227 microscope. Fluorescence bleaching at selected ROIs were carried out using a 488 nm
1228 laser line. Fluorescence intensities during recovery was quantified, and a representative
1229 graph plotting the normalized intensities is shown in **(C)** for control (DMSO treated) cells
1230 and **(D)** PC190723 treated cells. **(E)** Quantification of the half-time ($t_{1/2}$) values for control
1231 (N = 10) and PC190723 treated (N = 10) cells. Fluorescence recovery after
1232 photobleaching (FRAP) of **(F)** control (DMSO treated) and **(G)** PC190723 (56.2 μM)
1233 treated cells expressing HpFtsZ. Fission yeast cultures expressing HpFtsZ-GFP were
1234 imaged as mentioned above. Normalized fluorescence intensities of representative
1235 experiments are plotted for **(H)** control (DMSO treated) cells and **(I)** PC190723 treated
1236 cells. **(J)** Quantification of the half-time ($t_{1/2}$) values for control (N = 10) and PC190723
1237 treated (N = 10) cells. The $t_{1/2}$ values mentioned in the text were obtained by fitting the
1238 fluorescence recovery curves to a single exponential curve $F(t)= C(1 - e^{-kt})$ using Excel's
1239 Solver function and calculated from $t_{1/2} = \ln(2)/k$.
1240 An unpaired two-tailed Student's t-test was used to assess the statistical significance. P-
1241 values ≤ 0.0001 and ≤ 0.001 are indicated by **** and ***, respectively. The mean
1242 difference between the proportion of cells carrying FtsZ polymers in the untreated and
1243 treated populations is also indicated as effect size [95% CI, lower bound, upper bound].
1244 Scale bar represents 5 μm.
1245
1246

1247 **Figure 5. Determinants of resistance to PC190723 in HpFtsZ.** *S. pombe* cultures
1248 carrying HpFtsZ$^{WT}$, HpFtsZ$^{G213A}$ or HpFtsZ$^{T216E}$ were grown for 8 – 10 hours in the
1249 absence of PC190723 and then sub-cultured in the presence of the drug at 30°C for 4
1250 hours to allow the sufficient expression of the proteins and imaged using an
1251 epifluorescence microscope. While G213A is predicted to act as a steric block to
1252 PC190723, T216E would result in salt-bridge interactions with R326 (R307 in EcFtsZ$^{WT}$).
1253 **(A)** Effect of PC190723 on polymerization of HpFtsZ mutants G213A and T216E. The
1254 graph shows the percentage of cells having diffuse (light gray) and polymerized (dark
1255 gray) HpFtsZ in fission yeast in the absence (control) or presence of PC190723 (56.2 μM).
1256 Images showing the effect of PC190723 at 56.2 μM on **(B)** HpFtsZ$^{WT}$ (panel iv), **(C)**
1257 HpFtsZ$^{G213A}$ (panel iv) and **(D)** HpFtsZ$^{T216E}$ (panel iv). At a time-point when control
1258 (DMSO treated) cells expressing HpFtsZ$^{WT}$ show short polymers (panel ii), cells grown
1259 with PC190723 (56.2 μM) show stabilization of longer HpFtsZ polymers (panel iv).
1260 However, cells expressing **(C)** HpFtsZ$^{G213A}$ (panel iv) and **(D)** HpFtsZ$^{T216E}$ (panel iv)
1261 exhibit short polymers or diffuse fluorescence in the presence of 56.2 μM of PC190723 like
1262 in DMSO-treated cells expressing **(C)** HpFtsZ$^{G213A}$ (panel ii) and **(D)** HpFtsZ$^{T216E}$ (panel
1263 ii). The error bars shown are inferential and represent the 95% CI (N = 3). **** and ns
1264 indicate P-values ≤ 0.0001 and > 0.05 respectively. P-values were calculated from the
1265 two-sided proportions z-test. The mean difference between the proportion of cells carrying
1266 FtsZ polymers in the untreated and treated populations is also indicated as effect size
1267 [95% CI, lower bound, upper bound]. Scale bar represents 5 μm.
1268
1269

1270 **Figure 6. PC190723 can bind to the T state conformation of HpFtsZ. (A)** Overall
1271 structure of SaFtsZ bound to PC190723 (PDB ID: 4DXD; NBD - dark blue, H7 helix-
1272 magenta, T7 loop- purple and CTD- blue) with a zoomed-in view of PC190723 binding cleft
1273 (PDB ID: 4DXD; T state, open cleft) as inset. Residues of FtsZ, which interact with
1274 PC190723 (PDB ID- 4DXD), are shown in stick representation. **(B)** PC190723 binding cleft
1275 in R state conformation (PDB ID: 5H5I; sea green) is closed, and the residues clash with
1276 the drug (highlighted in black boxes) and prevent the binding of the drug. **(C)** HpFtsZ
1277 modelled in T state structure (light pink) and superimposed on PDB 4DXD. There are no
1278 clashes with the drug, and F281 could stack against the benzamide ring of PC190723.
1279 HpFtsZ does not possess any interaction that could potentially block the cleft. **(D)**
1280 PC190723 placed (by superposition of PDB 4DXD onto EcFtsZ T state model) in the
1281 pocket in EcFtsZ modelled in T state structure (green) highlight that there are two salt
1282 bridges, R307 and E198; D299 and R202 (shown in magenta and purple respectively) and
1283 a hydrogen bond between OH group of S227 and the main chain of G191 in H7 helix
1284 (shown in dark pink) which could block the cleft. **(E)** Residues in HpFtsZ and SaFtsZ
1285 corresponding to residues of EcFtsZ, which might block the PC binding cleft due to the
1286 three interaction types highlighted in the figure panels. In all panels, residues which are
1287 labelled in dark pink, magenta and purple fonts and boxed are the corresponding residues
1288 which form a salt bridge and hydrogen bonds in EcFtsZ. Dotted lines represent
1289 interactions at distances ≤ 4Å.

**Figure 1**

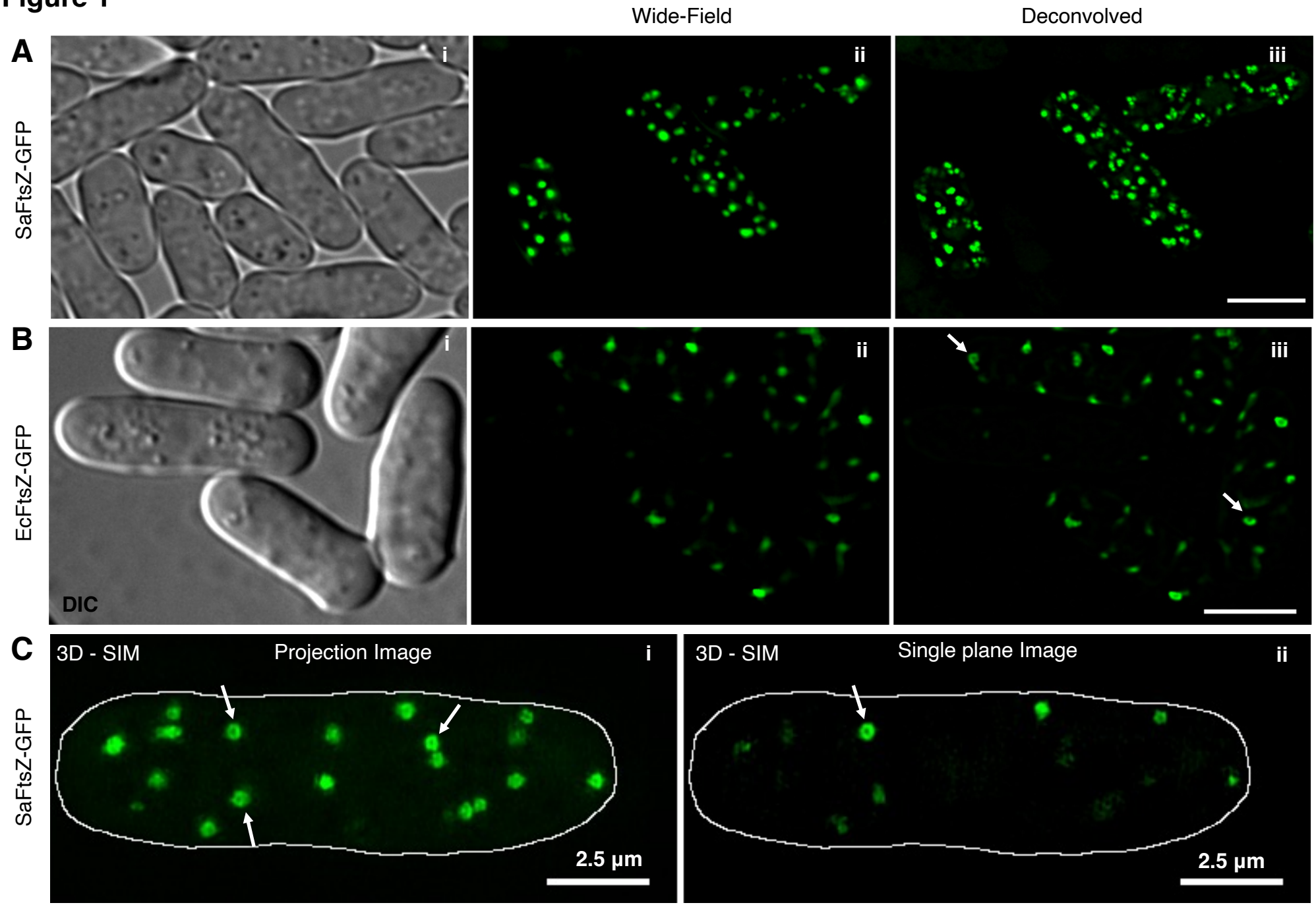
Wide-Field
Deconvolved
A
SaFtsZ-GFP
i
ii
iii
B
EcFtsZ-GFP
i
ii
iii
DIC
C
SaFtsZ-GFP
3D - SIM
Projection Image
i
2.5 µm
3D - SIM
Single plane Image
ii
2.5 µm

**Figure 1**

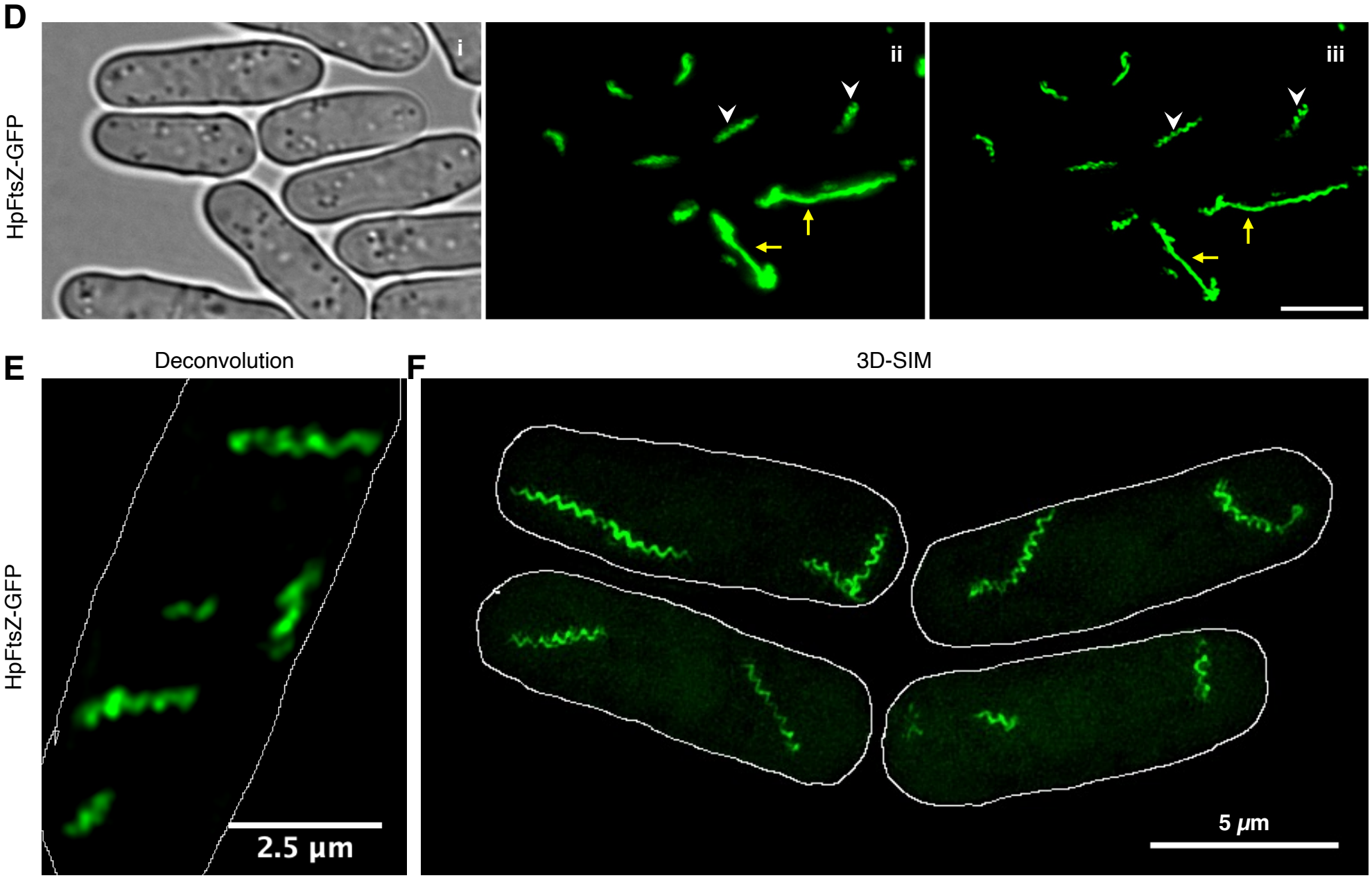
D
HpFtsZ-GFP
i
ii
iii
E
Deconvolution
HpFtsZ-GFP
2.5 µm
F
3D-SIM
5 µm

**Figure 2**

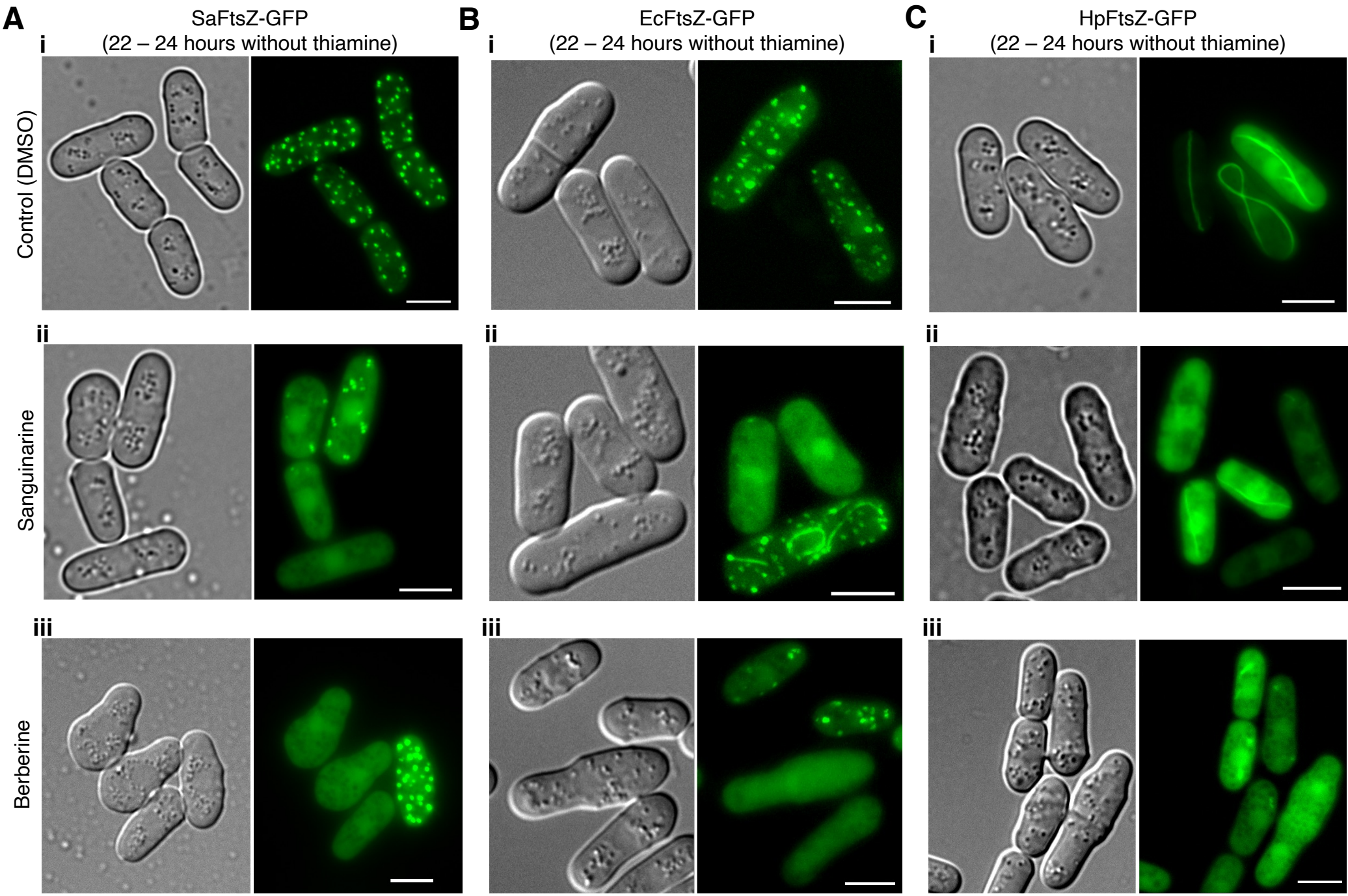
A
SaFtsZ-GFP
(22 – 24 hours without thiamine)
B
EcFtsZ-GFP
(22 – 24 hours without thiamine)
C
HpFtsZ-GFP
(22 – 24 hours without thiamine)
i
ii
iii
Control (DMSO)
Sanguinarine
Berberine

# Figure 2

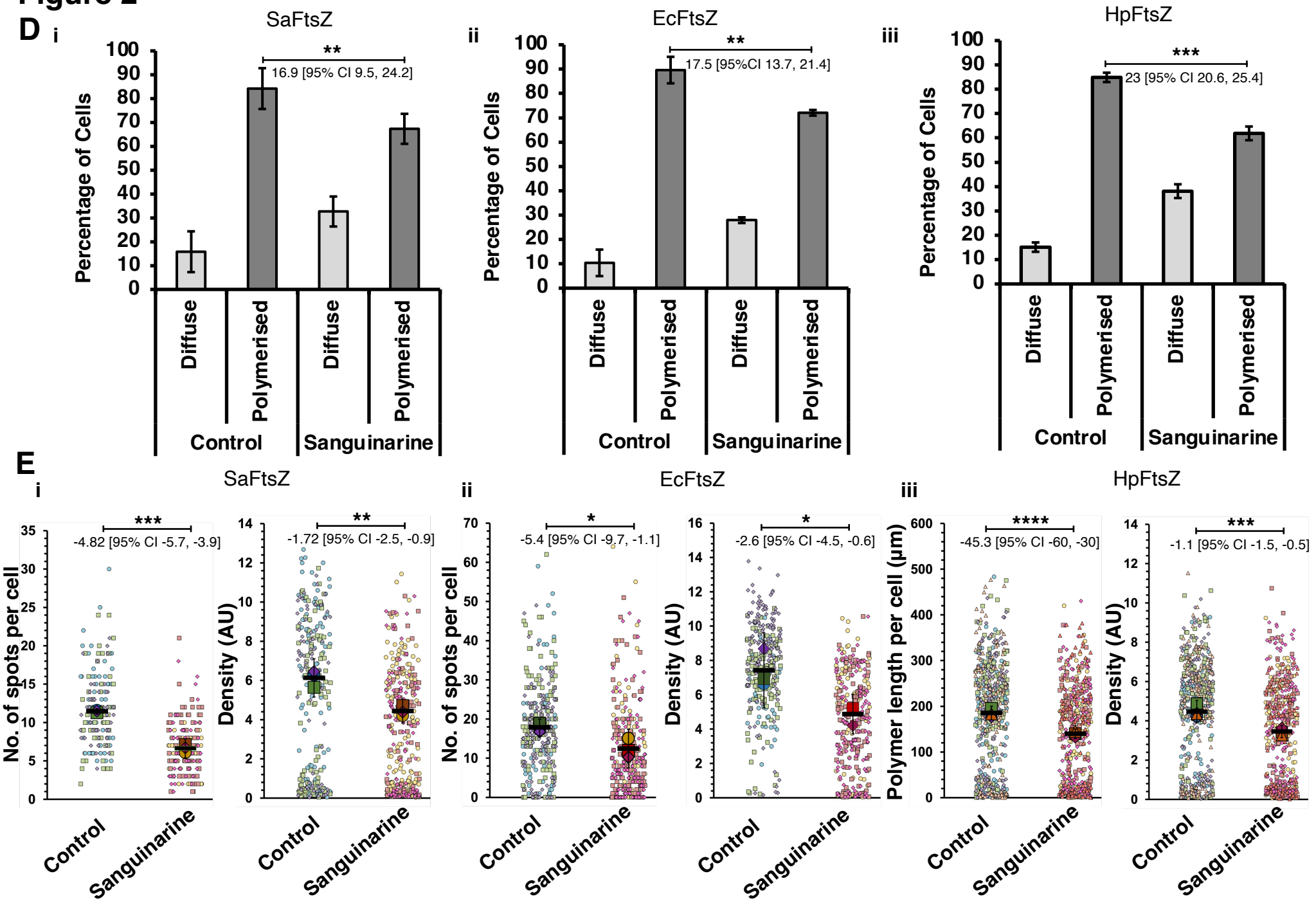
D
i
SaFtsZ
Percentage of Cells
**
16.9 [95% CI 9.5, 24.2]
Diffuse
Polymerised
Diffuse
Polymerised
Control
Sanguinarine
ii
EcFtsZ
**
17.5 [95%CI 13.7, 21.4]
iii
HpFtsZ
***
23 [95% CI 20.6, 25.4]
E
i
SaFtsZ
No. of spots per cell
***
-4.82 [95% CI -5.7, -3.9]
Density (AU)
**
-1.72 [95% CI -2.5, -0.9]
ii
EcFtsZ
*
-5.4 [95% CI -9.7, -1.1]
*
-2.6 [95% CI -4.5, -0.6]
iii
HpFtsZ
Polymer length per cell (µm)
****
-45.3 [95% CI -60, -30]
***
-1.1 [95% CI -1.5, -0.5]
Control
Sanguinarine

# Figure 2

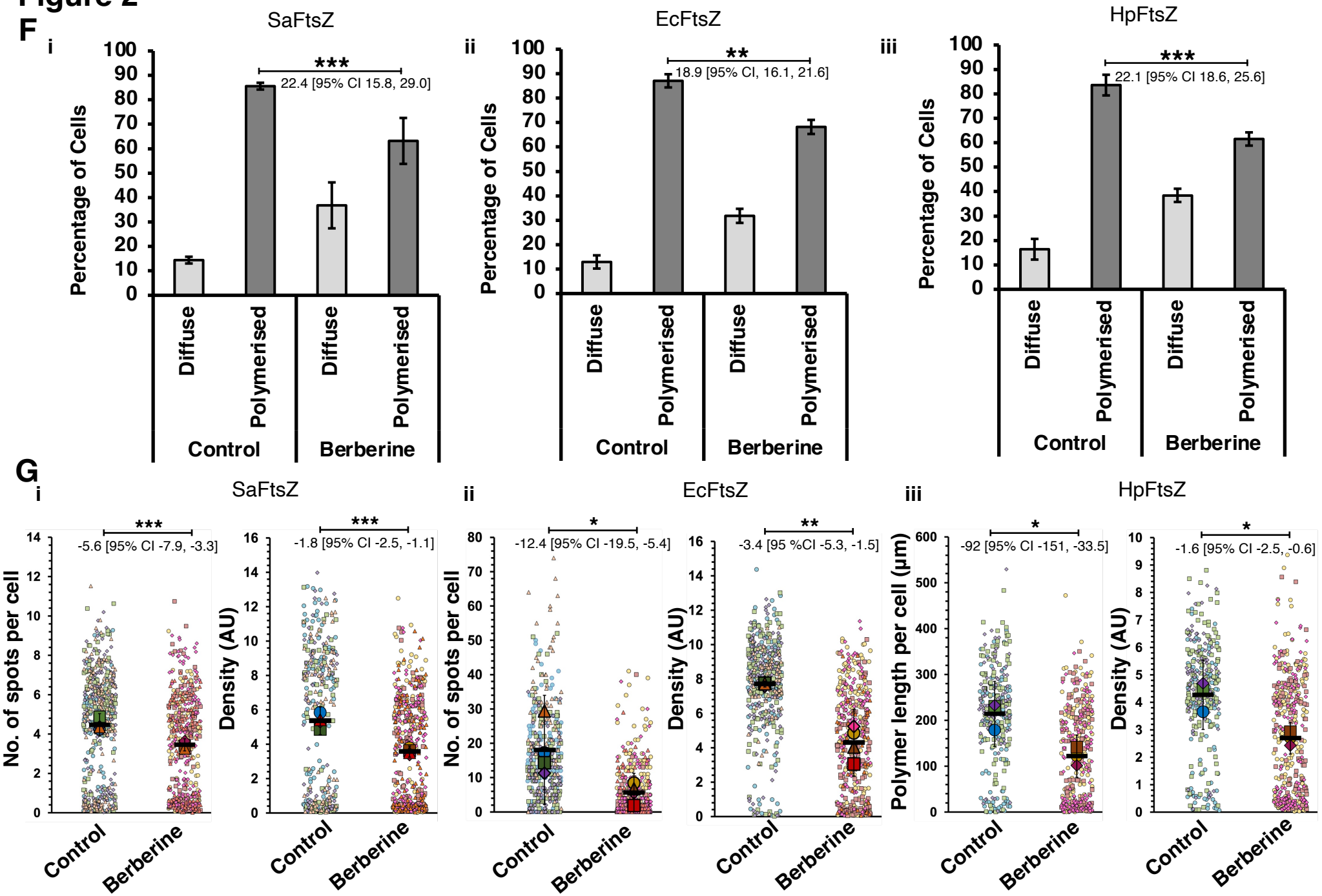
F
i
SaFtsZ
***
22.4 [95% CI 15.8, 29.0]
Percentage of Cells
Diffuse
Polymerised
Control
Berberine
ii
EcFtsZ
**
18.9 [95% CI, 16.1, 21.6]
iii
HpFtsZ
***
22.1 [95% CI 18.6, 25.6]
G
No. of spots per cell
-5.6 [95% CI -7.9, -3.3]
Density (AU)
-1.8 [95% CI -2.5, -1.1]
-12.4 [95% CI -19.5, -5.4]
-3.4 [95 %CI -5.3, -1.5]
Polymer length per cell (µm)
-92 [95% CI -151, -33.5]
-1.6 [95% CI -2.5, -0.6]

**Figure 2**

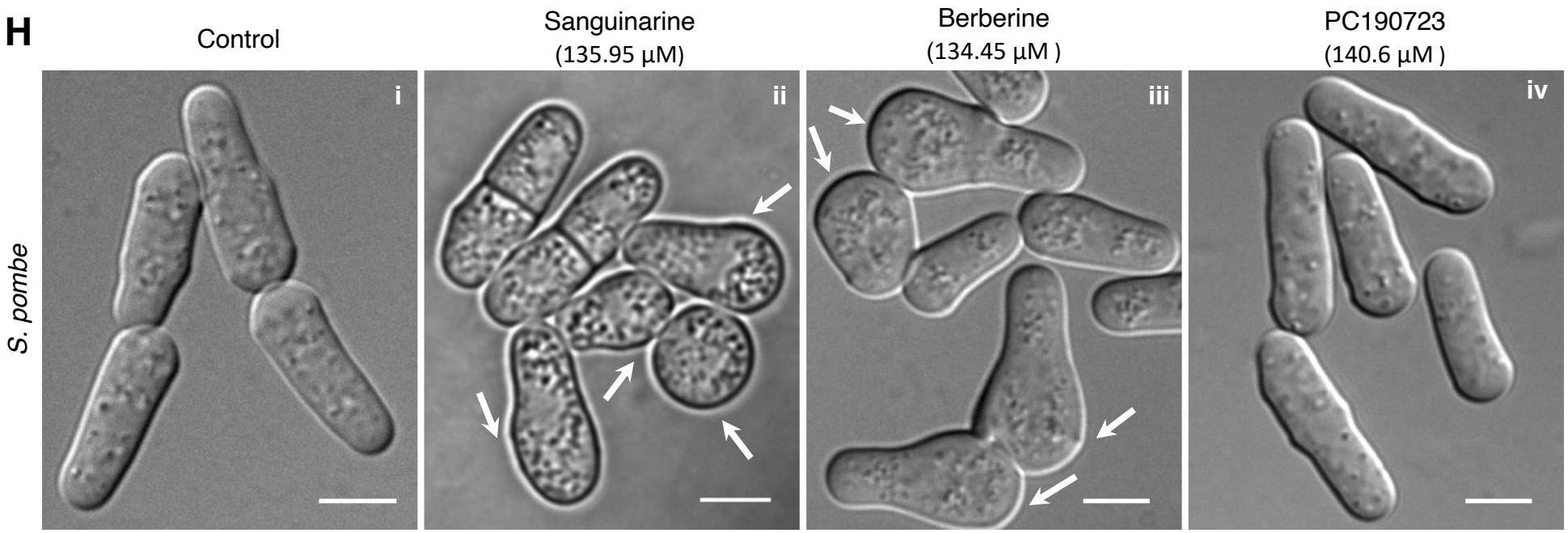
H
Control
Sanguinarine
(135.95 µM)
Berberine
(134.45 µM )
PC190723
(140.6 µM )
S. pombe
i
ii
iii
iv

Figure 3

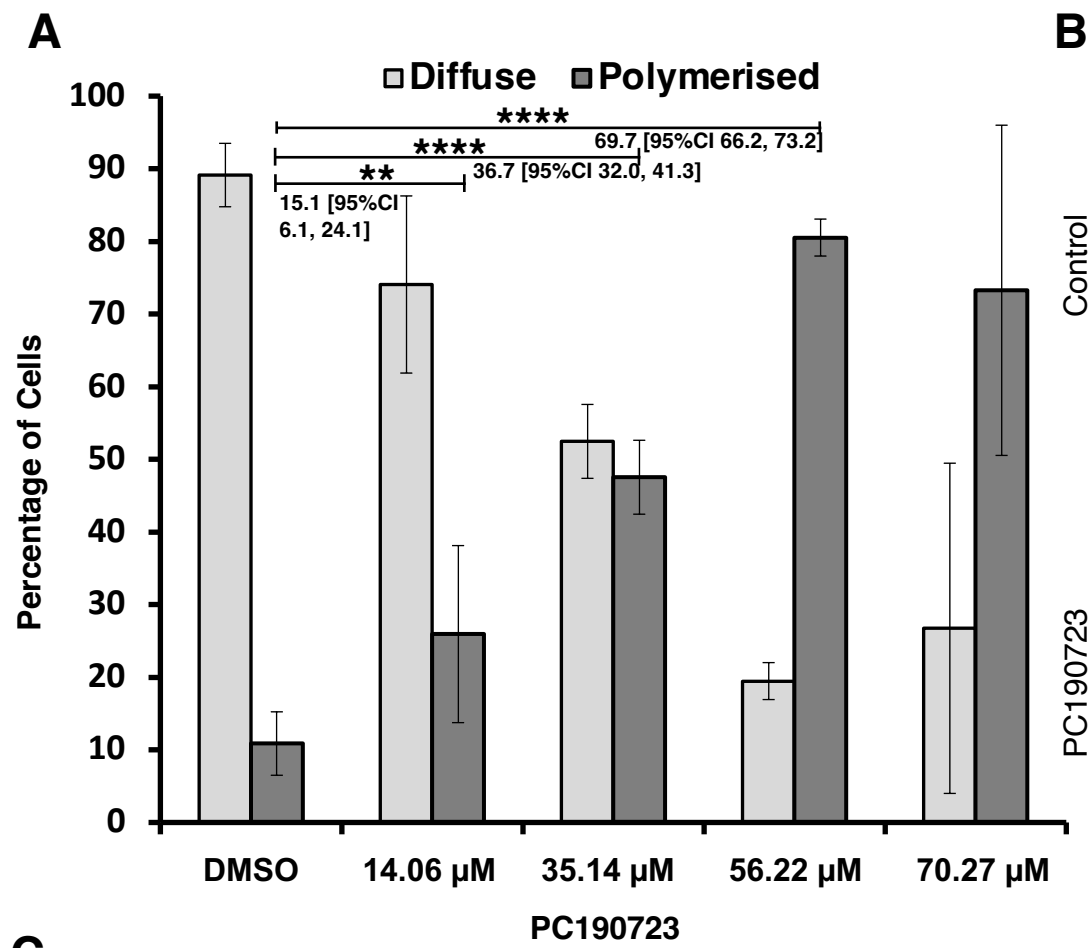
A
Diffuse
Polymerised
Percentage of Cells
100
90
80
70
60
50
40
30
20
10
0
****
****
**
69.7 [95%CI 66.2, 73.2]
36.7 [95%CI 32.0, 41.3]
15.1 [95%CI 6.1, 24.1]
DMSO
14.06 µM
35.14 µM
56.22 µM
70.27 µM
PC190723

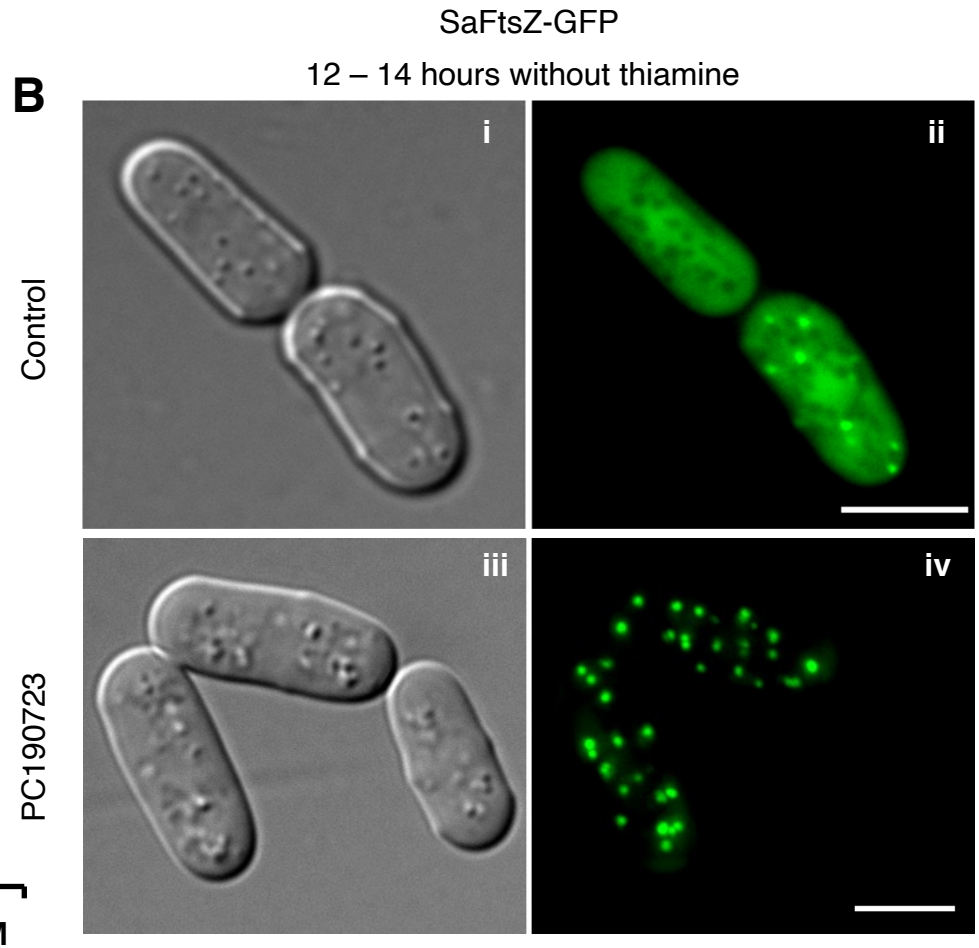
SaFtsZ-GFP
12 – 14 hours without thiamine
B
Control
PC190723
i
ii
iii
iv

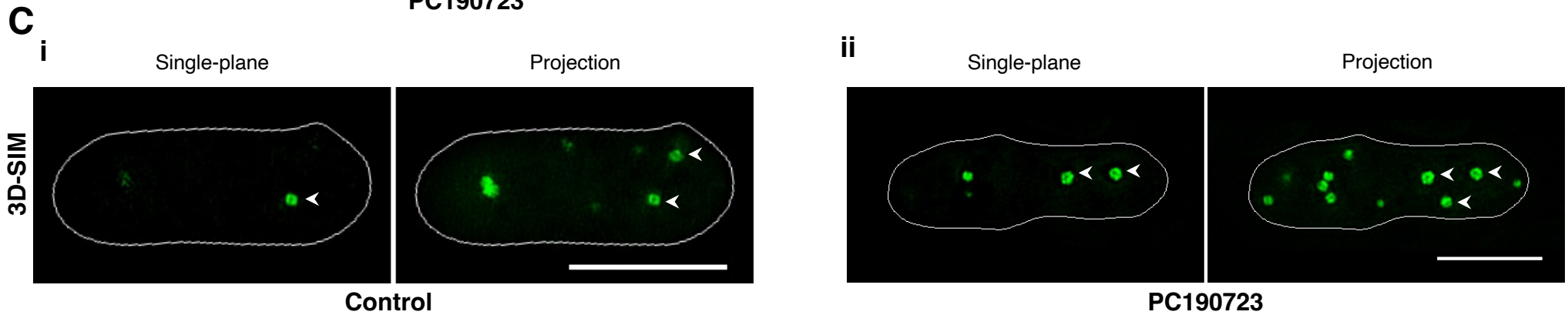
C
i
Single-plane
Projection
3D-SIM
Control
ii
Single-plane
Projection
PC190723

Figure 3

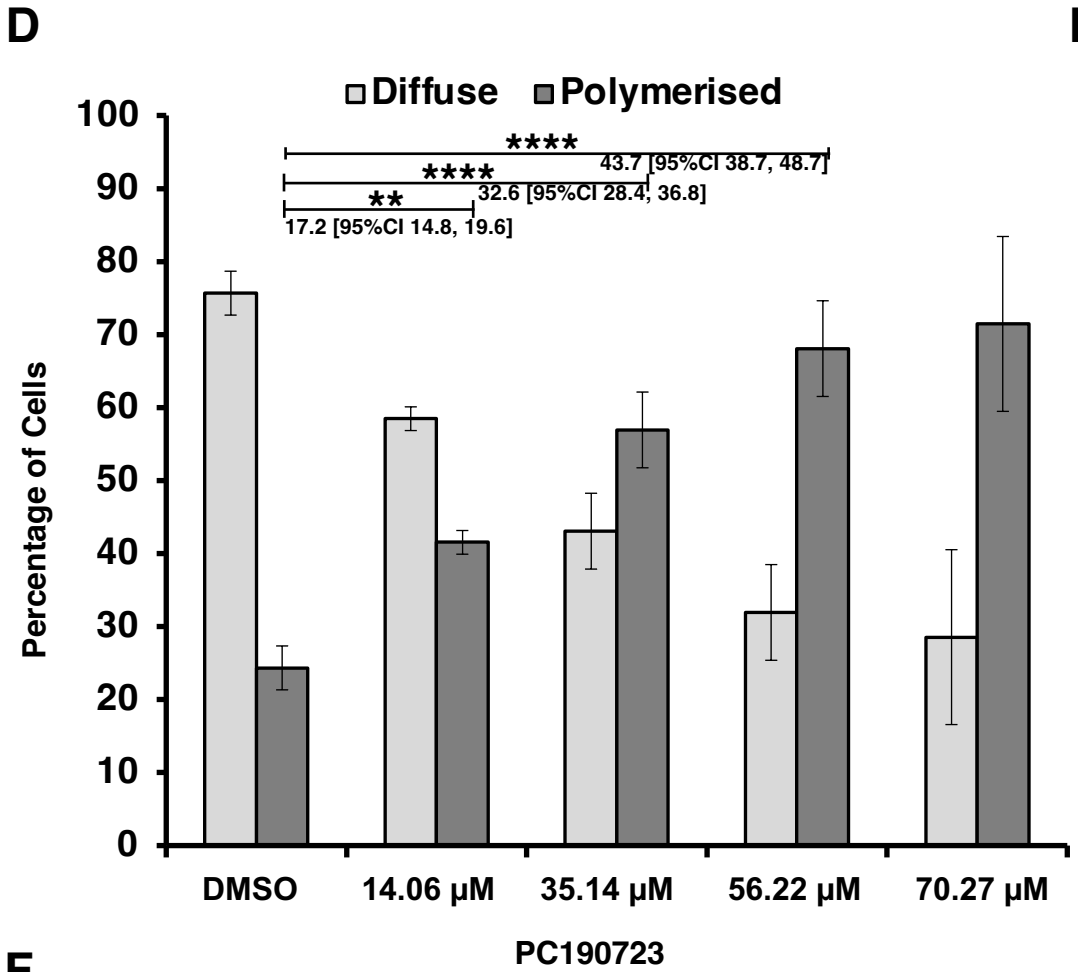
D
Diffuse
Polymerised
Percentage of Cells
100
90
80
70
60
50
40
30
20
10
0
****
43.7 [95%CI 38.7, 48.7]
****
32.6 [95%CI 28.4, 36.8]
**
17.2 [95%CI 14.8, 19.6]
DMSO
14.06 µM
35.14 µM
56.22 µM
70.27 µM
PC190723

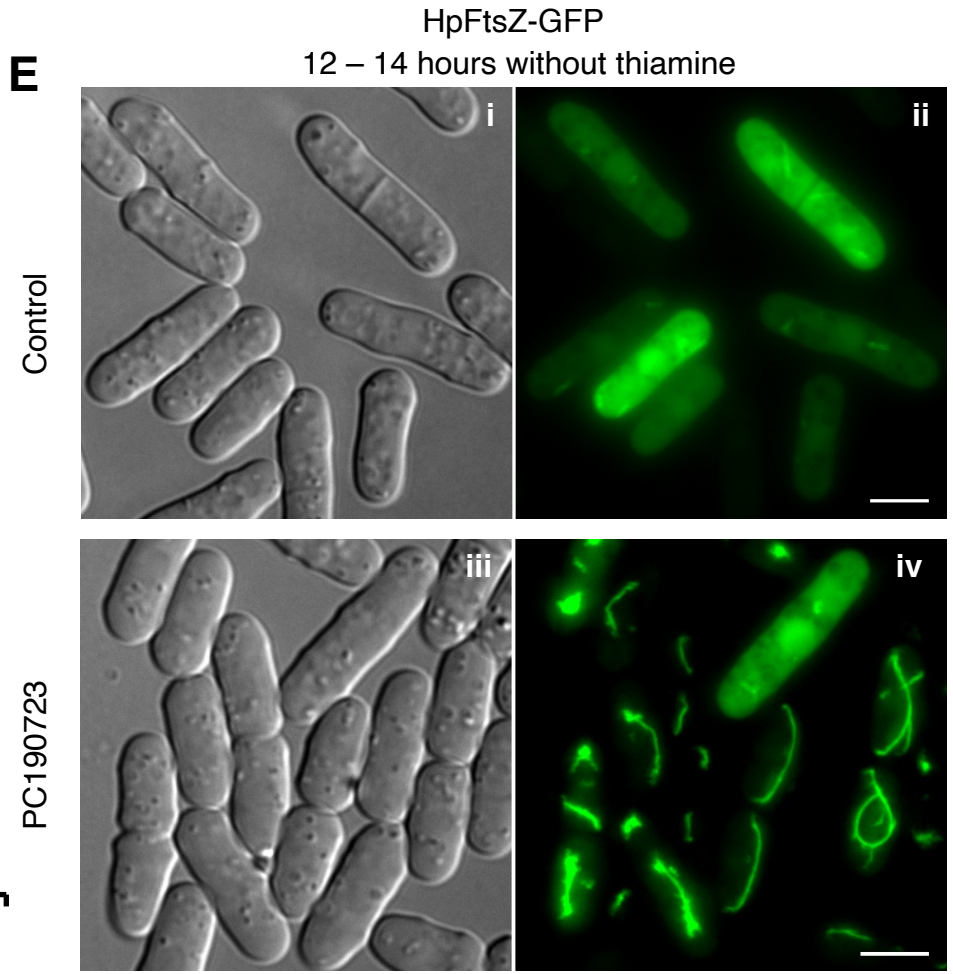
E
HpFtsZ-GFP
12 – 14 hours without thiamine
Control
PC190723
i
ii
iii
iv

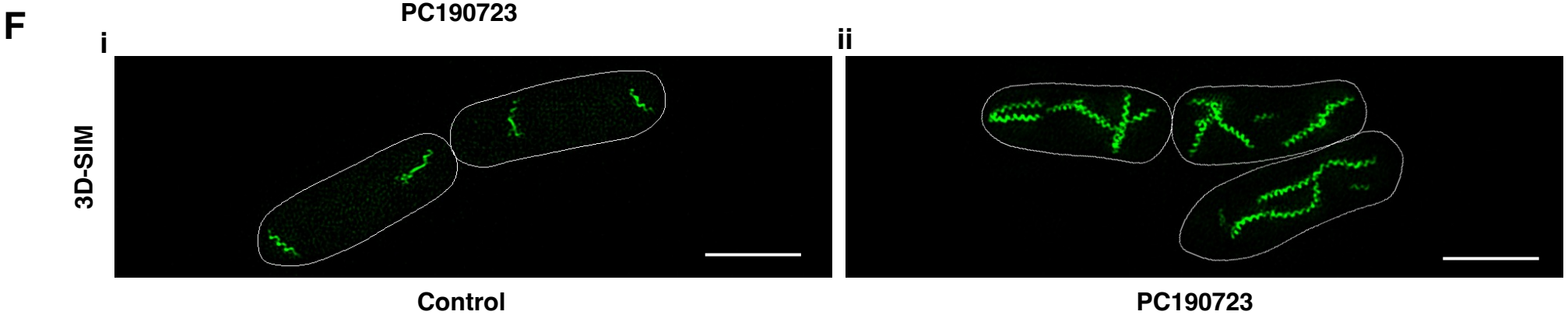
F
i
ii
3D-SIM
Control
PC190723

# Figure 3

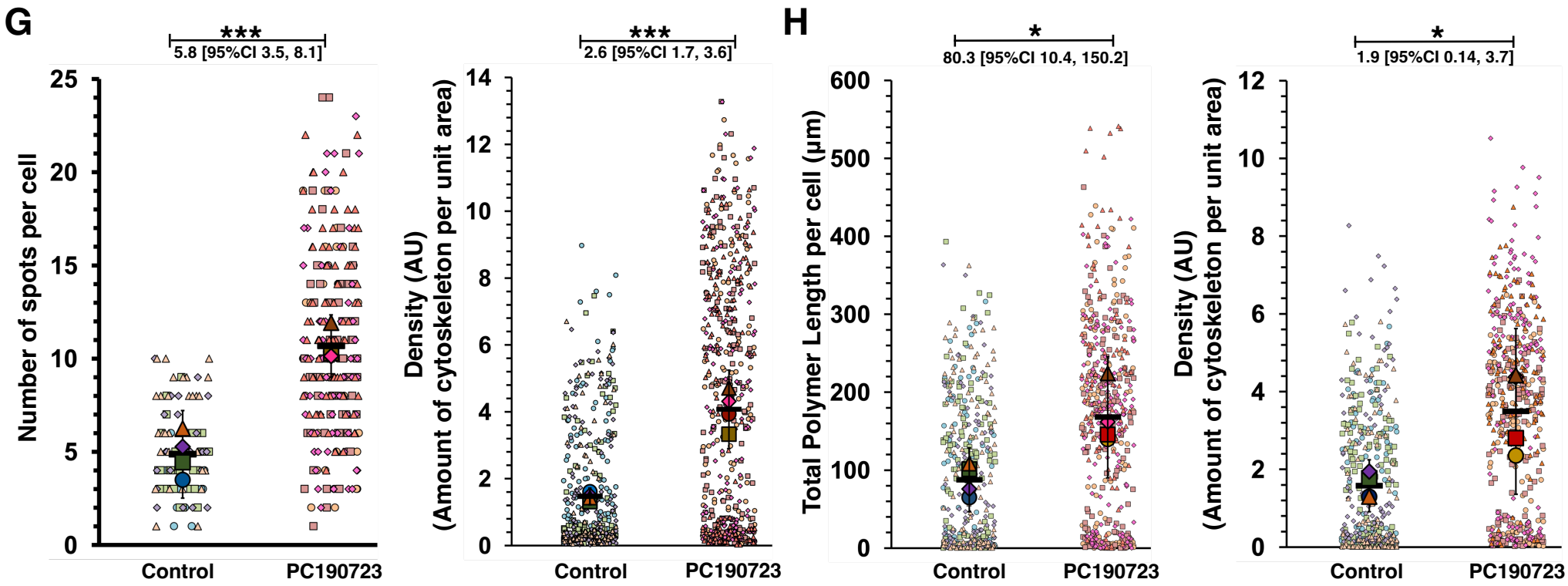
G
***
5.8 [95%CI 3.5, 8.1]
Number of spots per cell
Control
PC190723
***
2.6 [95%CI 1.7, 3.6]
Density (AU)
(Amount of cytoskeleton per unit area)
Control
PC190723
H
*
80.3 [95%CI 10.4, 150.2]
Total Polymer Length per cell (µm)
Control
PC190723
*
1.9 [95%CI 0.14, 3.7]
Density (AU)
(Amount of cytoskeleton per unit area)
Control
PC190723

# Figure 3

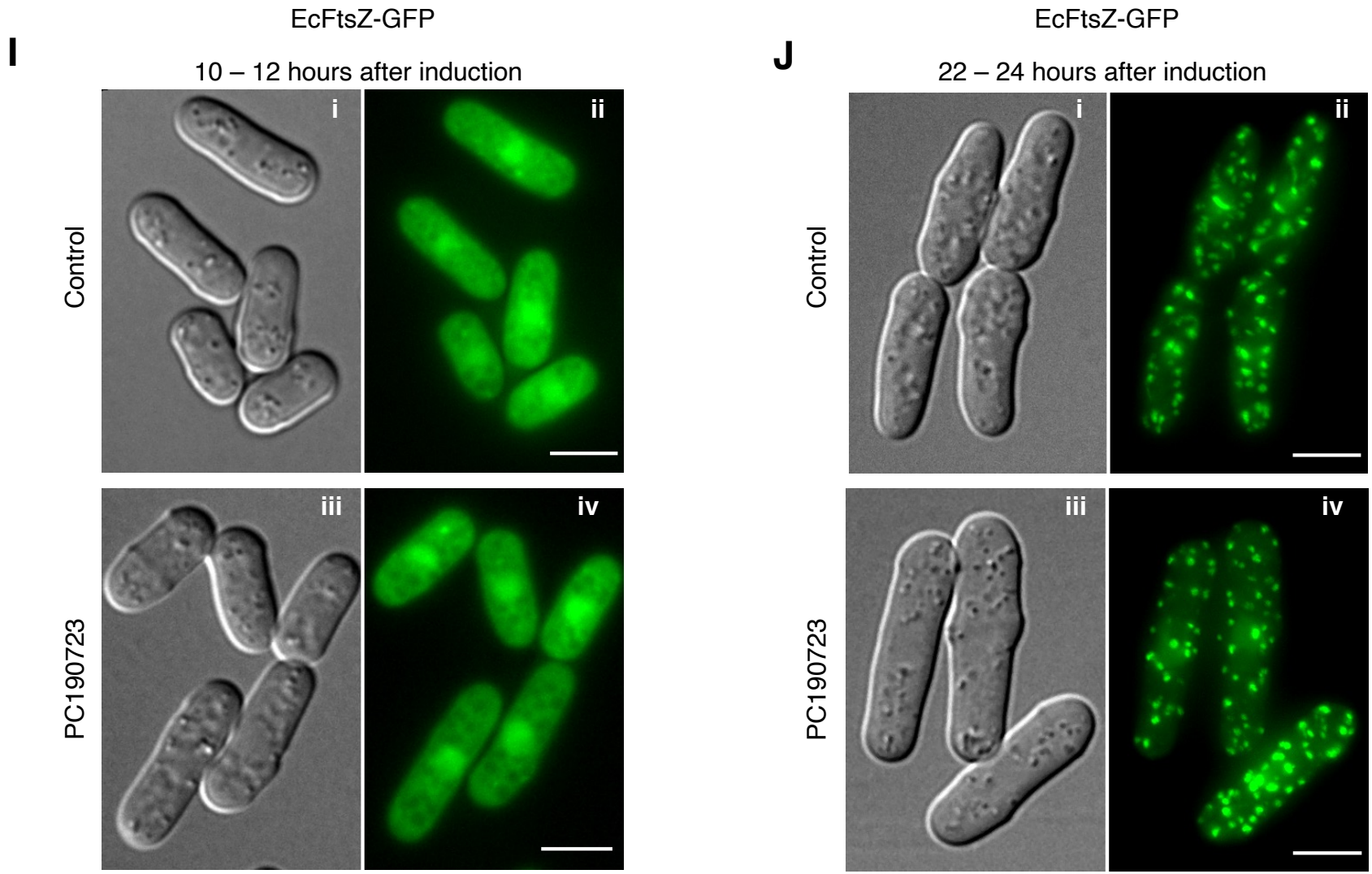
I
EcFtsZ-GFP
10 – 12 hours after induction
Control
PC190723
i
ii
iii
iv
J
EcFtsZ-GFP
22 – 24 hours after induction
Control
PC190723
i
ii
iii
iv

Figure 4

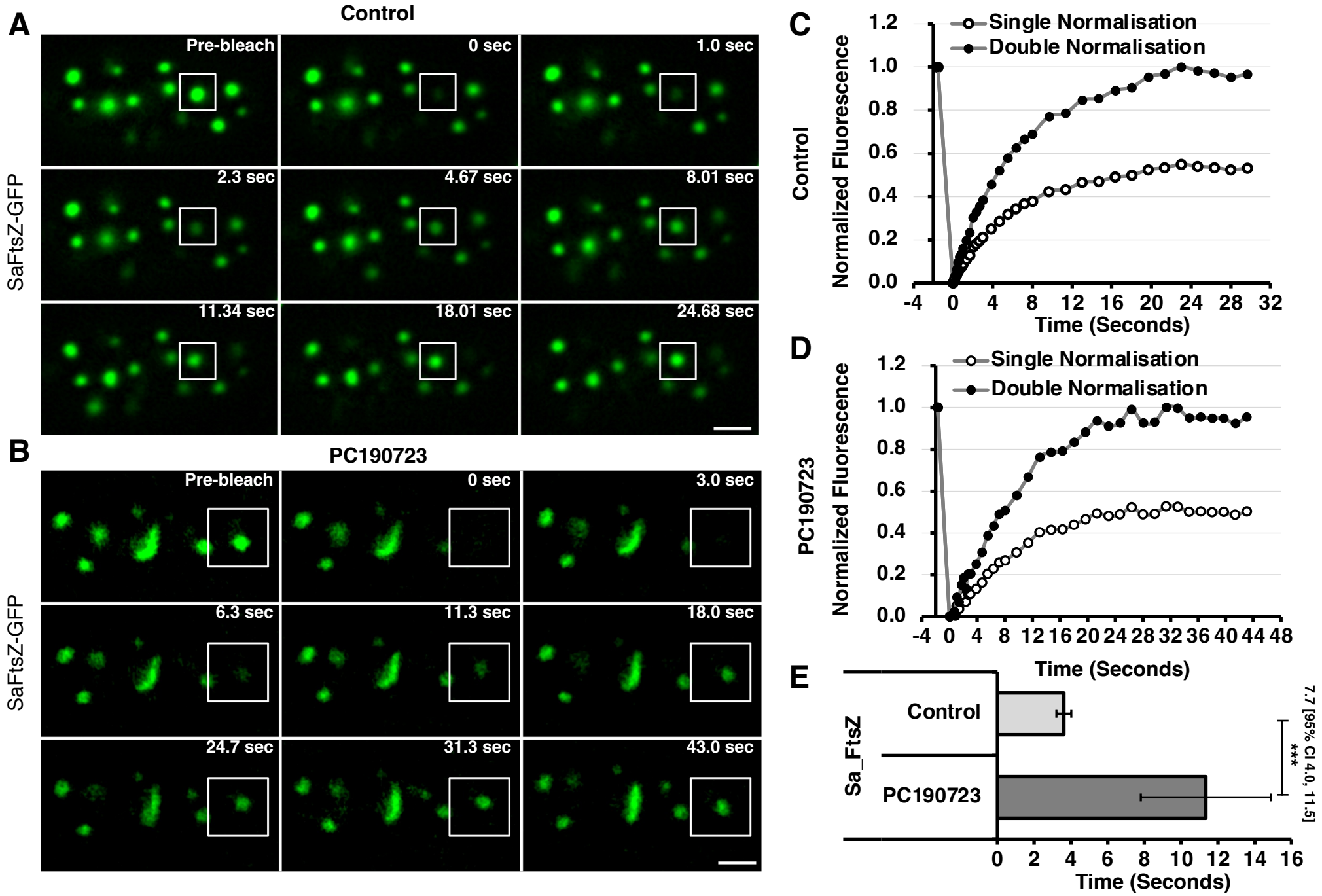
A
Control
SaFtsZ-GFP
Pre-bleach
0 sec
1.0 sec
2.3 sec
4.67 sec
8.01 sec
11.34 sec
18.01 sec
24.68 sec
B
PC190723
SaFtsZ-GFP
Pre-bleach
0 sec
3.0 sec
6.3 sec
11.3 sec
18.0 sec
24.7 sec
31.3 sec
43.0 sec
C
Control
Single Normalisation
Double Normalisation
Normalized Fluorescence
Time (Seconds)
D
PC190723
Single Normalisation
Double Normalisation
Normalized Fluorescence
Time (Seconds)
E
Sa_FtsZ
Control
PC190723
***
7.7 [95% CI 4.0, 11.5]
Time (Seconds)

Figure 4

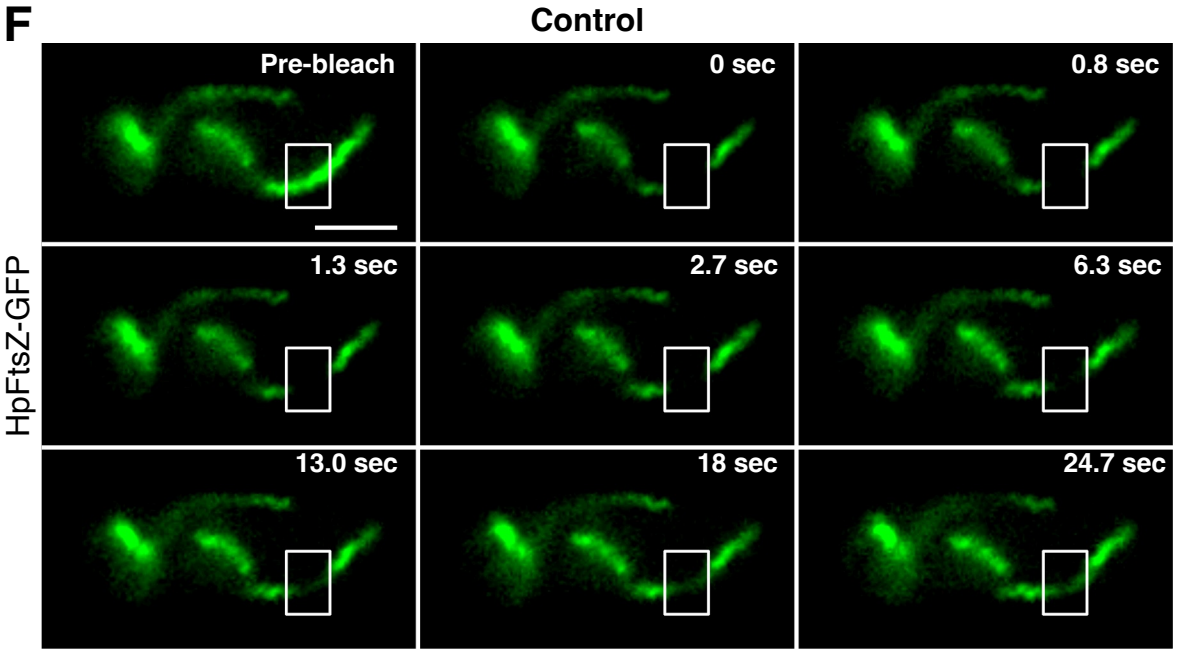
F
Control
HpFtsZ-GFP
Pre-bleach
0 sec
0.8 sec
1.3 sec
2.7 sec
6.3 sec
13.0 sec
18 sec
24.7 sec

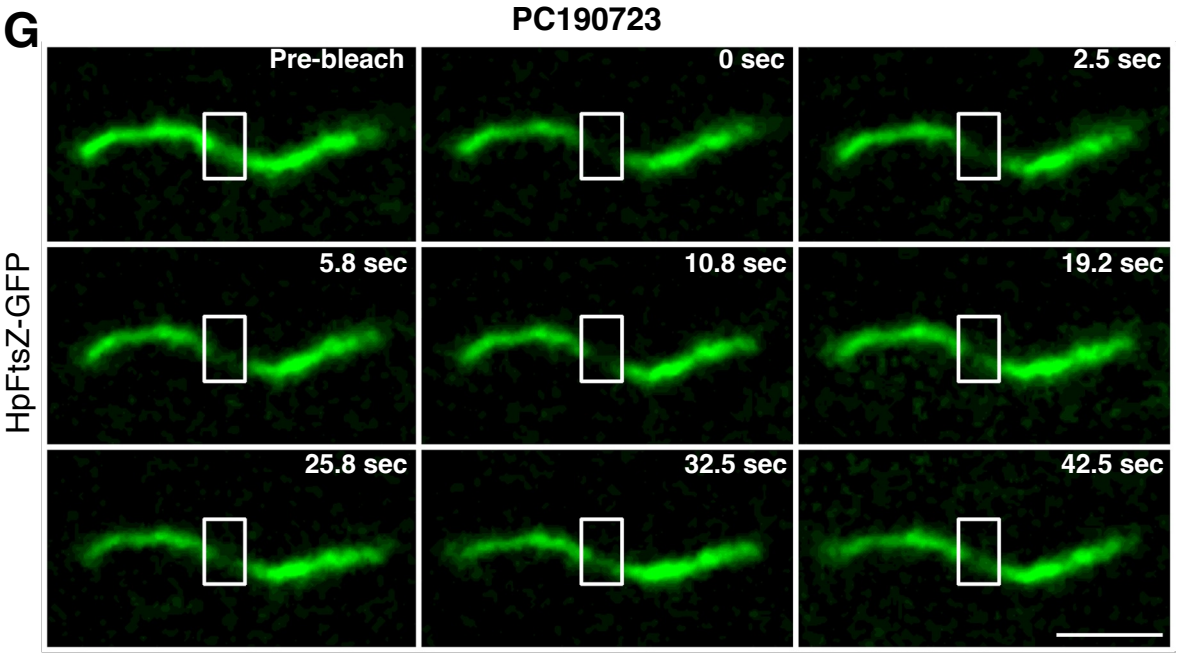
G
PC190723
HpFtsZ-GFP
Pre-bleach
0 sec
2.5 sec
5.8 sec
10.8 sec
19.2 sec
25.8 sec
32.5 sec
42.5 sec

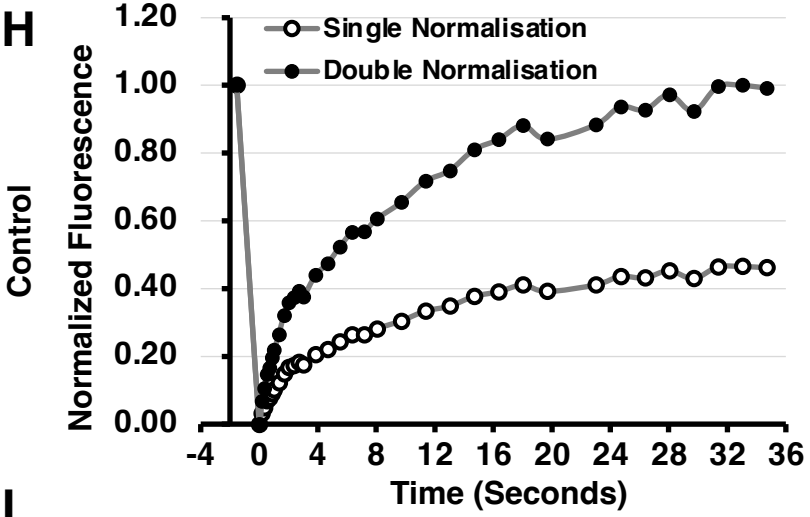
H
Control
Single Normalisation
Double Normalisation
Normalized Fluorescence
1.20
1.00
0.80
0.60
0.40
0.20
0.00
-4 0 4 8 12 16 20 24 28 32 36
Time (Seconds)

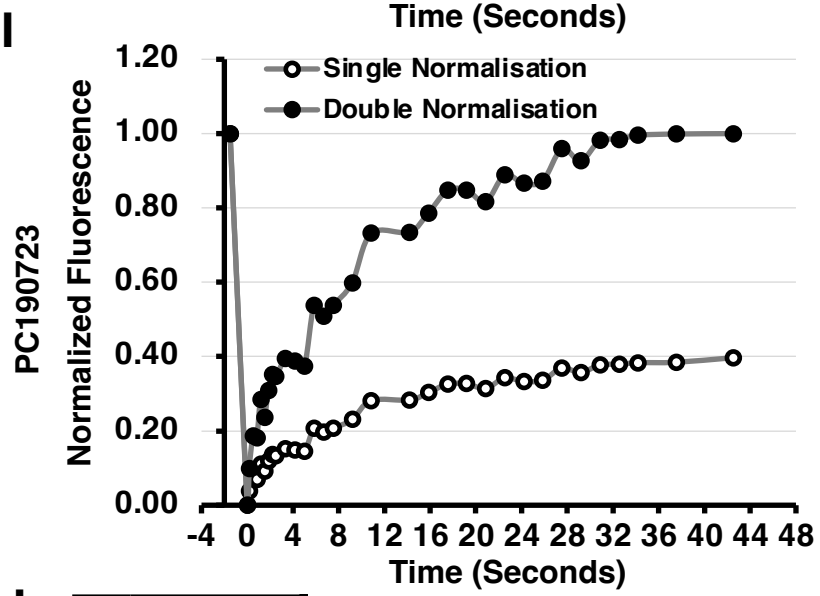
I
PC190723
Single Normalisation
Double Normalisation
Normalized Fluorescence
1.20
1.00
0.80
0.60
0.40
0.20
0.00
-4 0 4 8 12 16 20 24 28 32 36 40 44 48
Time (Seconds)

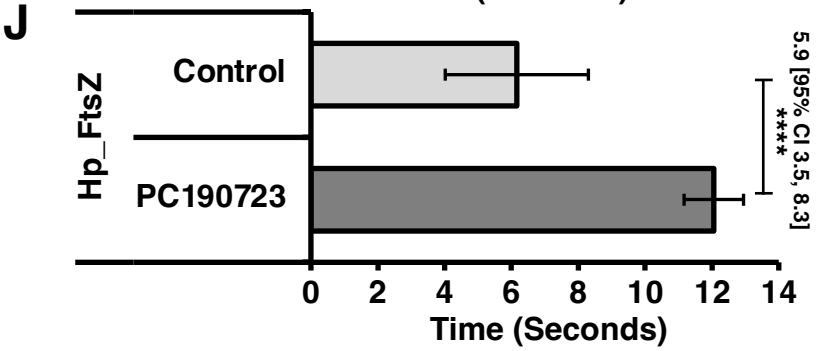
J
Hp_FtsZ
Control
PC190723
5.9 [95% CI 3.5, 8.3]
****
0 2 4 6 8 10 12 14
Time (Seconds)

Figure 5

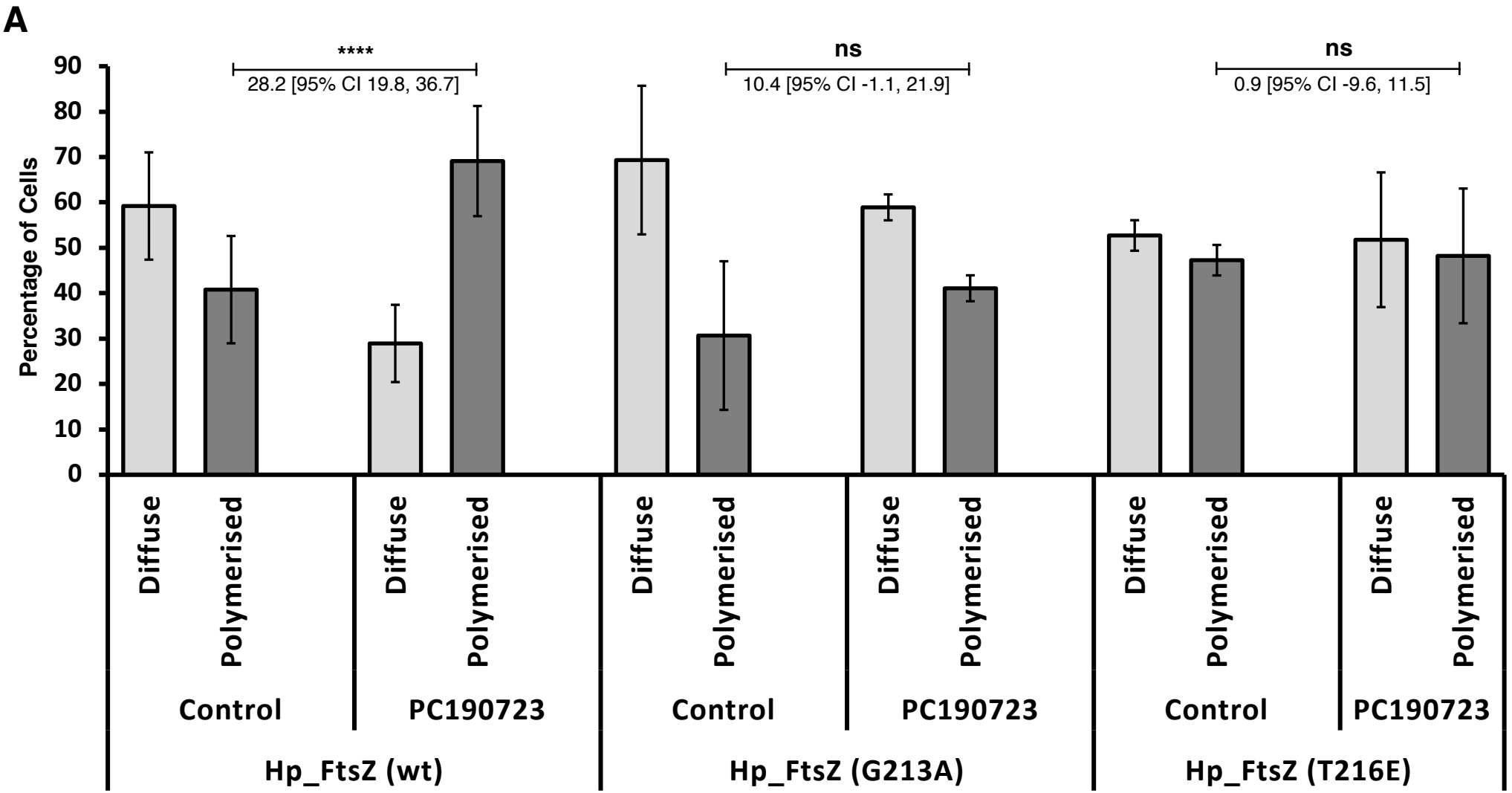
A
****
28.2 [95% CI 19.8, 36.7]
ns
10.4 [95% CI -1.1, 21.9]
ns
0.9 [95% CI -9.6, 11.5]
Percentage of Cells
90
80
70
60
50
40
30
20
10
0
Diffuse
Polymerised
Control
PC190723
Hp_FtsZ (wt)
Hp_FtsZ (G213A)
Hp_FtsZ (T216E)

**Figure 5**

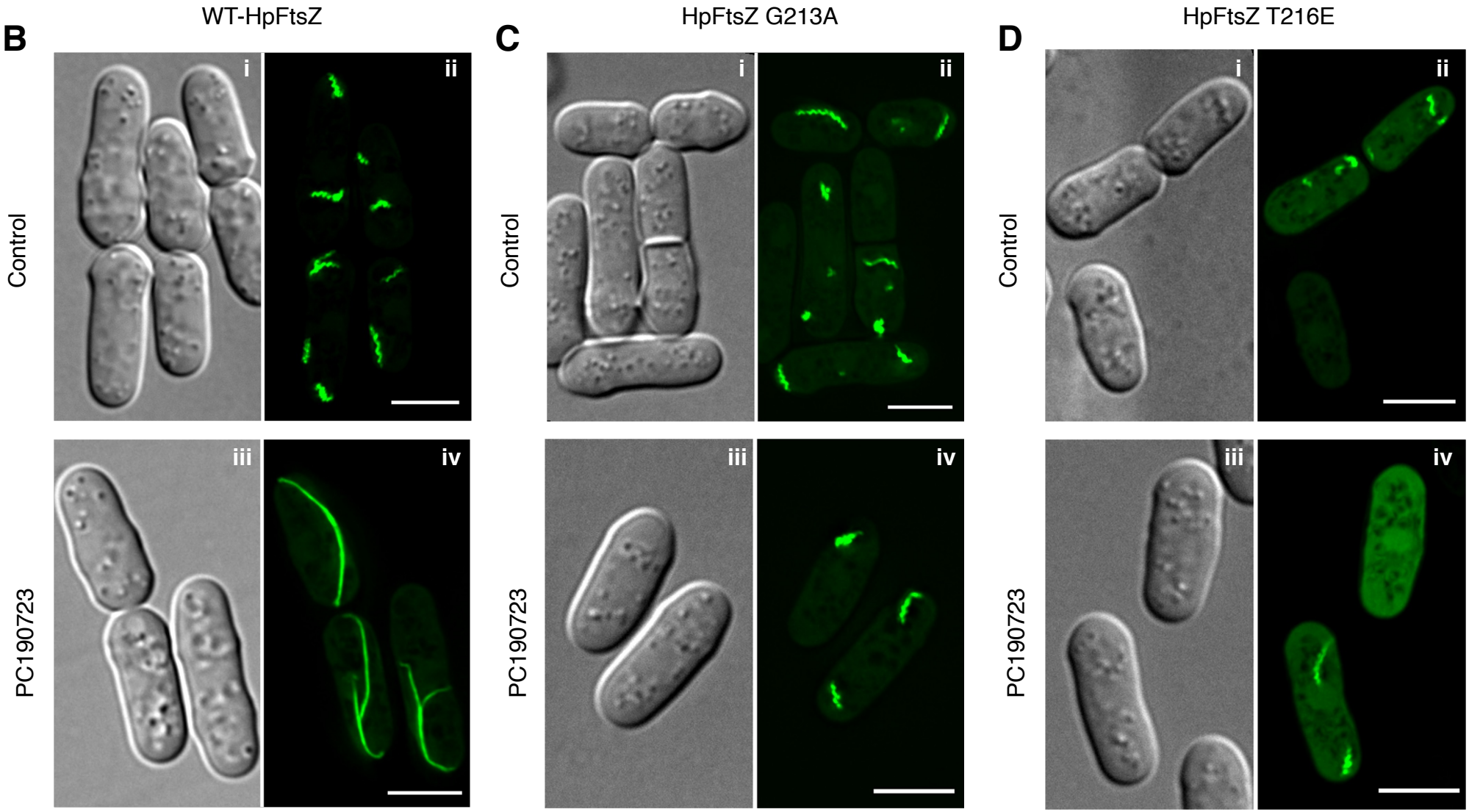
B
WT-HpFtsZ
C
HpFtsZ G213A
D
HpFtsZ T216E
Control
PC190723
i
ii
iii
iv

# Figure 6

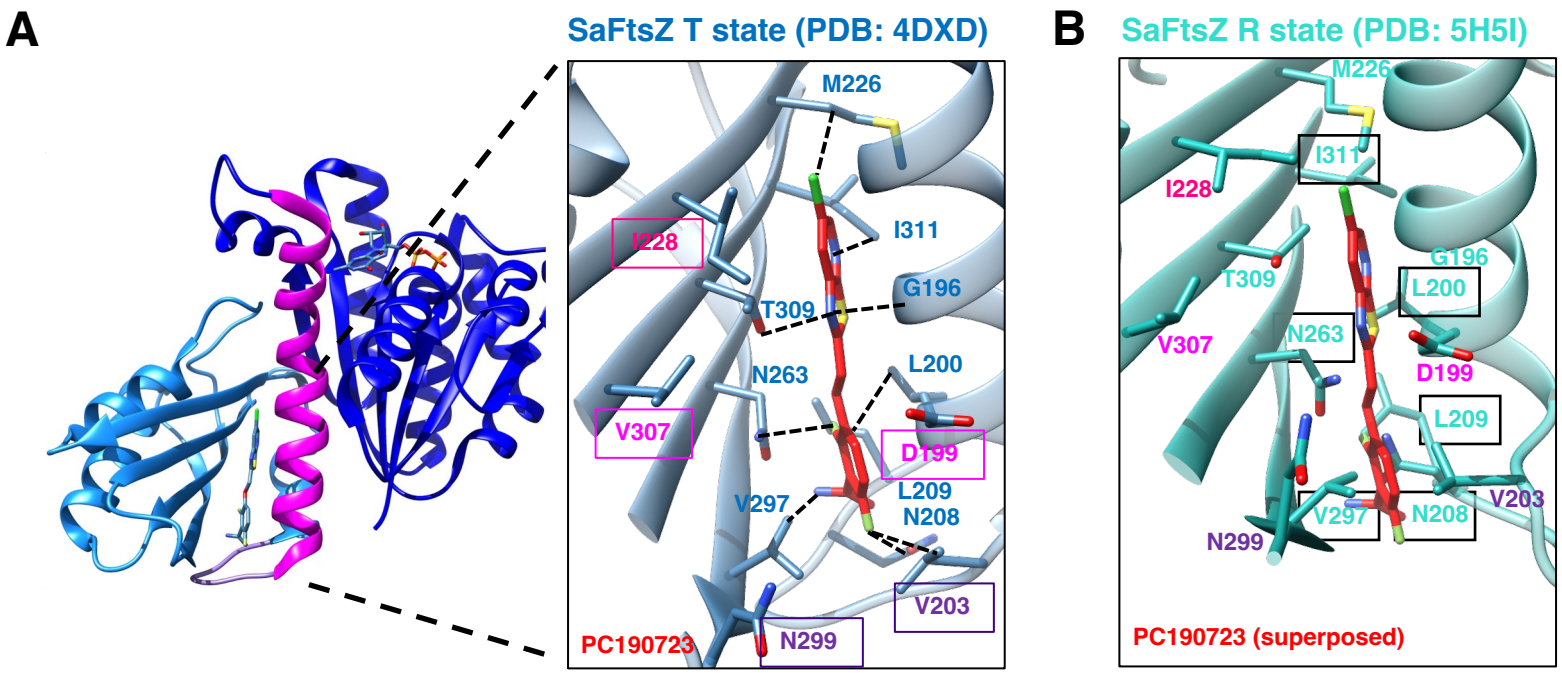


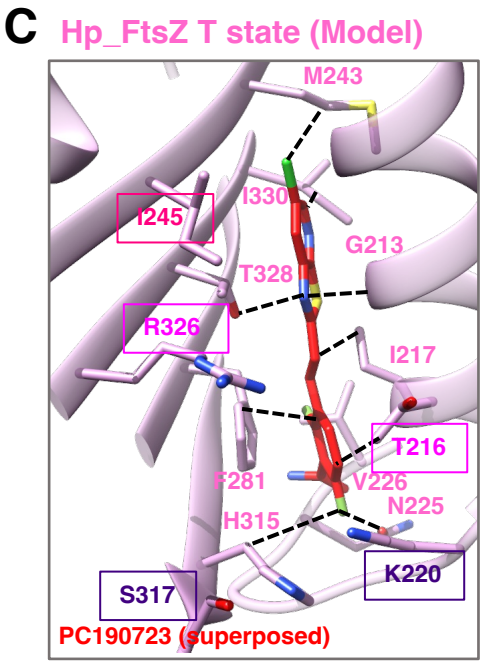


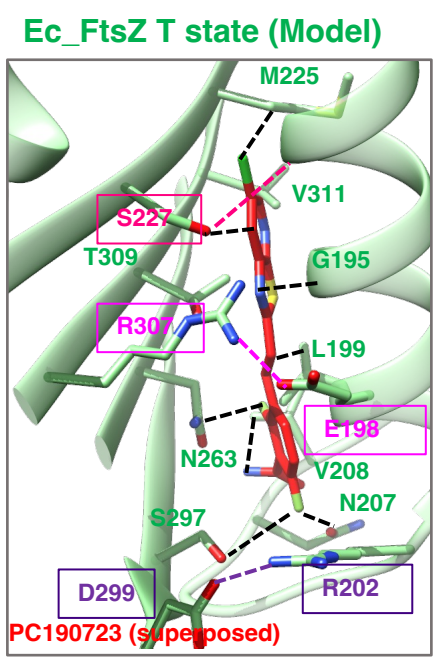


**E**

**Interaction 1 (Hydrogen bond)**

| | | | | |
|---|---|---|---|---|
| *H.pylori* | G I G | 246 | No | |
| *E.coli* | G S G | 228 | Yes | |
| *S.aureus* | G I G | 229 | No | |
| *B.subtilis* | G I G | 229 | No | |

**Interaction 2 (Salt Bridge)**

| | | | | | | |
|---|---|---|---|---|---|---|
| *H.pylori* | S T I | 217 | V R V | 327 | No |
| *E.coli* | A E L | 199 | L R V | 308 | Yes |
| *S.aureus* | S D L | 200 | I V V | 308 | No |
| *B.subtilis* | S D L | 200 | I V V | 308 | No |

**Interaction 3 (Salt bridge)**

| | | | | | | |
|---|---|---|---|---|---|---|
| *H.pylori* | T K P | 221 | T S D | 318 | No |
| *E.coli* | T R P | 203 | L D P | 300 | Yes |
| *S.aureus* | A V S | 204 | I N P | 300 | No |
| *B.subtilis* | A T P | 204 | I N E | 300 | No |